RSC Sustainability

ROYAL SOCIETY OF CHEMISTRY

PAPER

View Article Online
View Journal | View Issue

Cite this: *RSC Sustainability*, 2025, **3**, 5204

Molecular modelling of a biochar–ZnO–CuO nano-biofertilizer: adsorption simulation for optimized nutrient delivery

Adewale T. Irewale, [ab] Elias E. Elemike, [ac] Christian O. Dimkpa [b] and Emeka E. Oguzie *[a]

Amid growing concerns regarding the safety, efficacy, and environmental impact of conventional fertilizers, nanotechnology-based alternatives—particularly nano-biofertilizers—have emerged as promising solutions. In this study, we optimized a conceptualized biochar (CBC) structure (with formula: $C_{60}H_{39}NO_{13}$ and molar mass: 981.97 g mol^{-1}), building on both our ongoing research and existing literature. Molecular dynamics (MD) simulations were employed to investigate biochar adsorption interactions with zinc oxide (ZnO) and copper oxide (CuO) nanonutrients (NNs), as single and co-adsorbates. Quantitative computational analysis revealed that the CBC molecule exhibits structural stability, with a heat of formation of −226.45 kcal mol^{-1}, a total energy of −12,586.15 eV, and an ionization potential of 8.37 eV. Additional evaluations—including COSMO sigma profiling, UV-Vis spectral analysis, and frontier molecular orbital (HOMO–LUMO) mapping—gave deeper insight into CBC molecular properties. Distinct spatial separation of these orbitals across different functional groups underscores biochar's chemical stability, despite a small HOMO–LUMO energy gap (ΔE_{gap} = 0.058106 eV). Adsorption simulations demonstrated energetically favorable interactions between both NNs and CBC, with a higher affinity for CuO over ZnO (average rigid adsorption energy: −17.64 *vs.* −14.15 eV). The average structural deformation energy associated with ZnO compared to CuO in the adsorption process (−687.68 eV *vs.* −6.38 eV) shows different mechanisms or sites of adsorption, respectively. In the co-presence of both nanonutrients, energy parameters were modulated, indicating a positive synergy. These findings offer foundational insights into the molecular properties and thermodynamic behavior of biochar in nanonutrient adsorption. However, recognizing that real world factors such as soil cation exchange capacity, pH, microbiome, and humidity also influence these adsorption interactions, the study discusses their potential effects and recommends the need for further research to bridge theoretical models with empirical data, optimize nanoformulations, assess ecological impacts, and evaluate the economic viability of biochar-based nanofertilizers for sustainable agricultural applications.

Received 4th August 2025
Accepted 27th August 2025

DOI: 10.1039/d5su00646e

rsc.li/rscsus

Sustainability spotlight

This ongoing research explores the use of invasive water hyacinth to develop biochar-based, nano-enabled fertilizers aimed at advancing precision agriculture and environmental sustainability. By further integrating computational simulations, the study provides atomic-scale insights into how biochar interacts with nanoscale nutrients like ZnO and CuO, helping to optimize nutrient delivery and improve plant nutrient use efficiency. These efforts directly contribute to key UN Sustainable Development Goals (SDGs). For instance, the development of slow-release fertilizers supports SDG 2 (Zero Hunger) by reducing nutrient losses and enhancing food security. Biochar's strong carbon sequestration potential and nutrient retention capabilities also align with SDG 13 (Climate Action) by lowering greenhouse gas emissions and minimizing fertilizer runoff. The preferential adsorption of CuO over ZnO informs more efficient material design, supporting SDG 12 (Responsible Consumption and Production). Additionally, the stability of the biochar structure enhances nutrient retention and reduces leaching, contributing to SDG 6 (Clean Water and Sanitation). Finally, valorizing invasive biomass like water hyacinth helps manage aquatic ecosystems by preserving biodiversity, thereby supporting SDG 14 (Life Below Water). Overall, this study provides a molecular framework for designing sustainable biochar-based fertilizers that balance agricultural productivity with environmental stewardship.

[a]*Nanotechnology Research Group, Africa Center of Excellence in Future Energies and Electrochemical Systems (ACEFUELS), Federal University of Technology, Owerri, Nigeria. E-mail: emeka.oguzie@futo.edu.ng*

[b]*Department of Analytical Chemistry, The Connecticut Agricultural Experiment Station, New Haven, Connecticut 06511, USA*

[c]*Department of Chemistry, Federal University of Petroleum Resources Effurun, Nigeria*

1. Introduction

Biochar (BC), a relatively stable carbonaceous material produced through the thermochemical treatment of biomass under low or no oxygen conditions, has recently garnered

significant attention from many researchers due to the widespread availability of feedstocks and its versatility in application.[1–3] BC can be produced from various sources such as rice husk,[4,5] wheat straw,[6] wood,[7] and water hyacinth,[3,8–10] making it both accessible and adaptable for different uses. Its role as a soil amendment and as a material for direct photosynthetic carbon capture and sequestration is well documented[10–14] with its nanostructures – such as high surface area and porosity – contributing significantly to its beneficial properties in soil amendment.[15,16]

Our recently published studies have experimentally characterized the physicochemical properties of water hyacinth-derived biochar, including surface area and pore volume analysis *via* Brunauer–Emmett–Teller (BET) measurements, using its CO_2 adsorption capacity.[16,17] However, experimental approaches to studying biochar are often hampered by time consuming processes and high energy requirements. In this current study, we applied molecular modeling techniques like molecular dynamics (MD) simulations to gain insights into the physicochemical aspects of BC. These simulations would provide reproducible and detailed atomistic information about BC's adsorption processes at the molecular level, which is crucial for optimizing biochar–nanonutrient formulations.[15,18]

The advent of nanotechnology has brought about transformative innovations to many fields. In agriculture, it includes nanofertilizers, nanopesticides, nanosensors and so forth.[19–25] In particular, nanofertilizers, with their engineered nutrient delivery systems, present promising solutions to the challenges of modern agriculture. Their effectiveness, however, depends on a thorough understanding of their adsorption dynamics at the molecular level.[26–30] The interactions between BC and nanoparticles are significantly influenced by BC intrinsic factors such as surface chemistry, pore structure, and charge, as well as extrinsic factors like soil pH, organic matter content, mineral composition, and water content.[31] A molecular-level understanding of these interactions is therefore critical for formulating efficient nanofertilizers that optimize nutrient delivery, enhance agricultural sustainability, and minimize environmental impacts.

At the core of these adsorption processes are the molecular interactions between nanofertilizer components and soil constituents, which ultimately determine the performance of biochar-based nanofertilizer systems.[32–34] This molecular-level understanding of adsorption dynamics in biochar-based nano-formulations is paramount for leveraging the full potential of nanotechnology in agricultural systems. Integrating interdisciplinary research with advanced analytical tools will enable the optimization of nanofertilizer design, addressing global food security challenges while safeguarding environmental health. The MD modeling is envisaged as a foundational guide in the process of nanoformulations as shown in Fig. 1. Reliance on efficient fertilizers in contemporary agriculture is germane as excessive use of conventional chemical fertilizers – especially nitrogen – has been linked to nutrient depletion and environmental degradation.[15]

For example, studies have shown that overuse of commercial inorganic fertilizers can result in the loss of up to 70% of potassium from the soil before crops even utilize it.[35] In contrast, nanofertilizers – comprising nanonutrients adsorbed onto matrix materials such as BC – offer a more environmentally friendly alternative through mechanisms that enable controlled and sustained nutrient release. This approach not only leads to significant cost savings but also supports more efficient, sustainable, and eco-friendly farming practices.[36–38] By

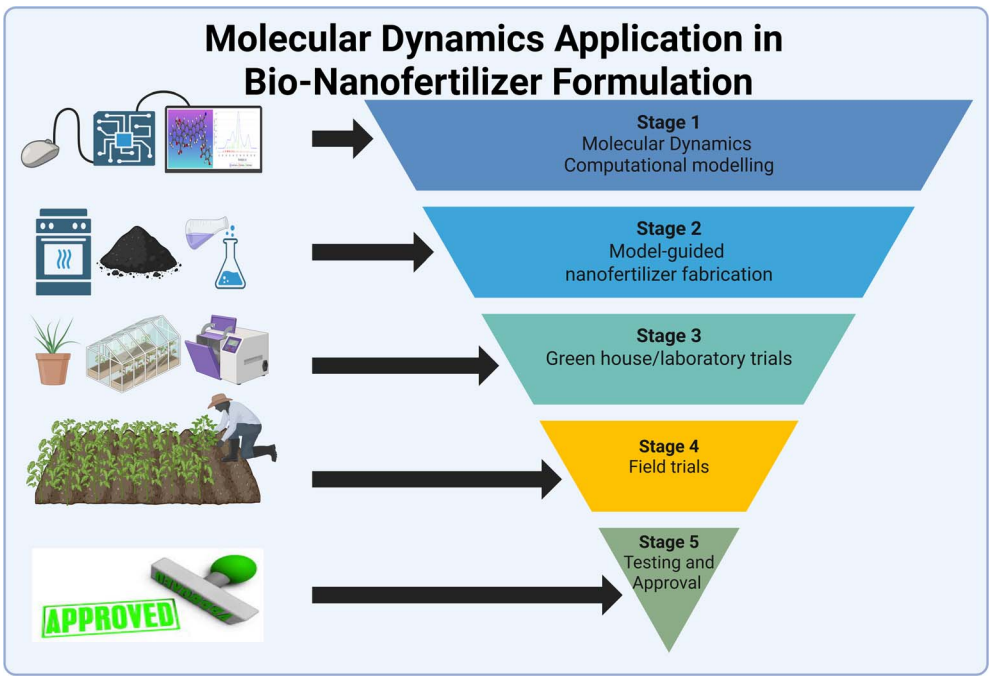

Fig. 1 Possible foundational application of molecular dynamics simulation in the bio-nanofertilizer formulation process.

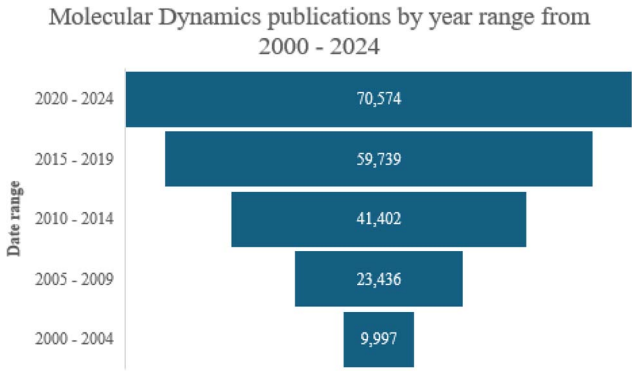

Fig. 2 Number of publications on molecular dynamics by the year range showing a progressive increase from 2000 to 2024. (Data generated from the PubMed database).

minimizing nutrient losses and environmental degradation, nanofertilizer technologies align with the core principle of sustainable development: meeting the needs of the present generation without compromising the ability of future generations to meet their own needs.[39]

However, despite the demonstrated utility of atomistic insights from MD simulations in materials science, these tools remain underutilized in the development of nano-enabled biochar-based fertilizers.[40] Modelling packages, such as BIOVIA Material Studio,[41,42] allow for the prediction, analysis, and optimization of material structures at the molecular level aiding in their specific design and synthesis using various modules under different preset ambient conditions. There are different computational simulations that can be applied depending on the type of material being modeled as well as the processes to be investigated. However, a quick metadata survey of publications in the PubMed database (U.S. National Center for Biotechnology Information) indicates that computational molecular dynamics (MD) has gained increasing popularity among researchers and material scientists since the early 2000s (2000–2024; Fig. 2). When the root term "molecular dynamics" was combined with modifiers such as "simulation", "biochar", "nanofertilizer", and "nano", the results revealed that MD remains largely unexplored in biochar–nanonutrient interactions at the atomistic scale. Notably, the search yielded 201 855 publications for "molecular dynamics" alone, but only 29 for its combination with "biochar," none with "nanofertilizer," and 5035 with "nano" (Fig. 3). This gap highlights the need for computational approaches to better understand nanonutrient adsorption and desorption processes, which could serve as valuable tools for cost-effective and time-efficient nanofertilizer formulations—similar to the advances already seen in molecular biology, drug discovery and design.[43,44]

Addressing this gap, the present study employed MD simulations to investigate how the intrinsic properties of BC influence its adsorption interactions with ZnO and CuO nanonutrients, using conceptualized biochar structures through Material Studio Suite software.[45] In our previous study,[16] we reported that biochar derived from water hyacinth obtained from Effurun, Nigeria, was deficient in zinc and copper. This observation informed the decision to focus on these two nanonutrients, given their essential roles as nutrients promoting plant health and vitality. The present work, therefore, aims to provide a deeper molecular-level understanding that can drive the rational design of next-generation, sustainable agricultural formulations. Although MD simulations offer significant potential for the rapid analysis and design of BC, there remains a critical need for models that strike a balance between simplicity and accuracy—effectively capturing the complex and heterogeneous nature of BC without excessive oversimplification. To mitigate this challenge, we have intentionally compared theoretical predictions with available experimental data wherever feasible, thereby strengthening the validity and reliability of our results. Furthermore, multiple modules within the Materials Studio suite were employed to internally validate computational outputs, using carefully chosen approximations to minimize potential errors.

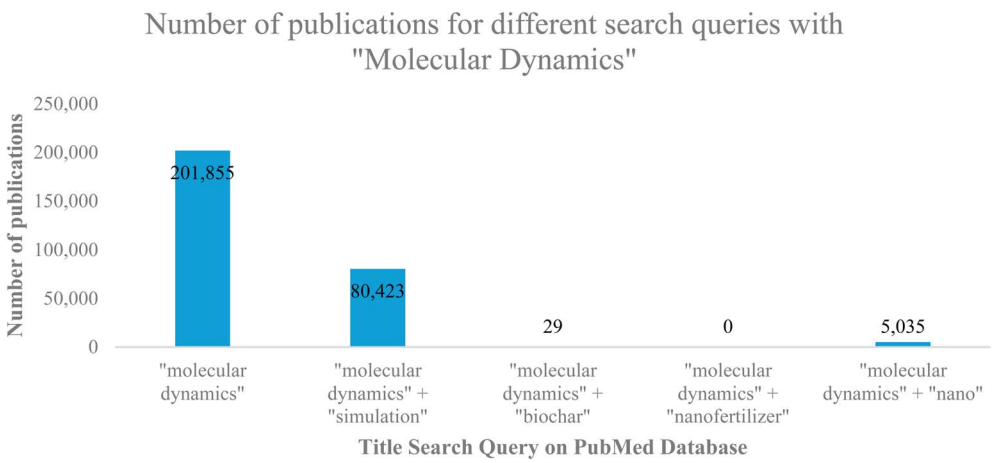

Fig. 3 Number of publications for different search queries with "molecular dynamics" as the root word alone and in combination with other modifiers as couplets. (Data generated from the PubMed database).

2. Computational methods

2.1 Conceptualized BC molecular structure

The production of BC typically yields a crude mixture of various heterogeneous BC species, with variations influenced by feedstock type, pyrolytic conditions, and pre- or post-treatment processes.[46–49] In this work, molecular dynamics (MD) computational modeling was performed using a conceptualized biochar (CBC) molecule, developed based on physicochemical data from our ongoing research[16,17] and structural models reported in the literature.[50–52] This approach enabled us to investigate the intrinsic molecular and atomistic properties of the CBC that can influence BC-nanonutrient adsorption phenomena – an essential factor in designing nanonutrient-fortified, biochar-based fertilizers. The optimized CBC structure, with a molecular mass of 981.97 g mol^{-1}, is presented in Fig. 4a and the energy minimization profiles in Fig. 4b. While BC is inherently heterogeneous, the CBC model was designed to reflect the dominant structural and chemical features consistently observed across diverse experimental studies. By incorporating key functional groups and molecular motifs found in a wide range of biochar samples and validating the model against both in-house and published data, we ensured that the CBC serves as a representative proxy for bulk or crude biochar, thereby minimizing potential faults associated with non-representativeness.

2.2 Nanonutrient adsorbates

The ZnO and CuO adsorbates were modeled as monomeric oxide molecules, each consisting of one metal atom (Zn or Cu) and one oxygen atom, forming optimized ZnO and CuO units, respectively (Fig. 5). This approach captures the essential interaction between a single nanonutrient and the biochar model, while maintaining computational efficiency. The bond lengths were initialized based on literature-reported values,[53] and all structures were fully optimized prior to adsorption simulation. This simplified model is widely used in DFT studies of metal oxide adsorption on carbon-based or porous materials[54–56] and is appropriate for isolating intrinsic binding and electronic effects without cluster-related complexities.

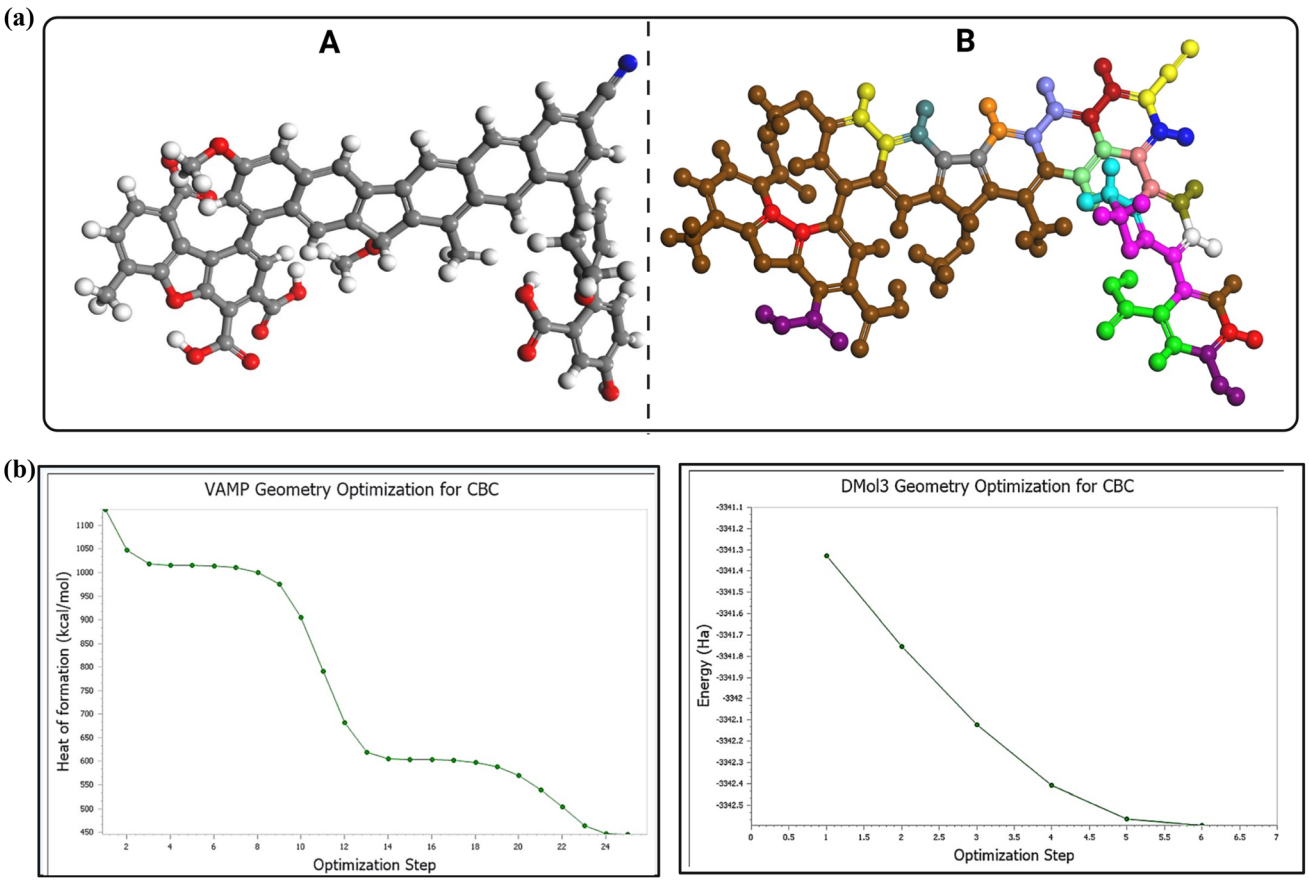

Fig. 4 (a) Optimized geometry for the conceptualized BC structure A = atom-based coloration, B = charged group-based coloration. A: oxygen = red, carbon = gray, hydrogen = white, and nitrogen = blue. B: brown = aromatic backbone or conjugated carbon rings; red = carbonyl or carboxylic acid groups; orange = electron-rich linkers or conjugated unsaturated groups; green = alkyl chains or hydrophobic moieties; purple = amino or nitrogen-containing side chains; cyan/blue-green = alcohol or ether groups; pink = amine or polar side groups; white = terminal hydrogens or methyl groups. (b) Geometry optimization profiles of the conceptualized biochar (CBC) structure using two computational methods. [VAMP (semi-empirical) showing the decrease in heat of formation over 25 optimization steps, and $DMol^3$ (DFT-based) showing rapid energy minimization within 6 steps. Both methods confirm convergence to a stable, low-energy configuration, with $DMol^3$ offering faster and more accurate optimization].

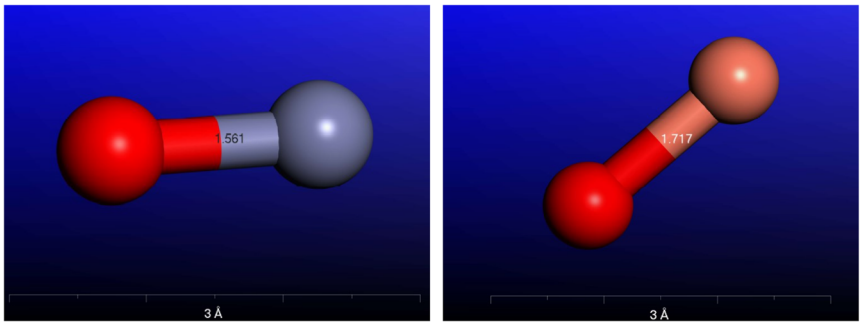

Fig. 5 ZnO and CuO molecules showing DMol^3-optimized bond lengths in Å.

2.3 Electronic structure calculations using VAMP

To complement the DFT-based DMol^3 simulations, the VAMP module in Material Studio software[45] (BIOVIA Material Science Studio Academic Research Suite – product no. 5CB-LUR, 2022) was employed to perform semi-empirical molecular orbital calculations based on the NDDO (Neglect of Diatomic Differential Overlap) approximation.[42] This is because compared to other geometry optimization techniques, VAMP includes several enhancements that enable it to successfully optimize even complex molecular systems, while offering features such as transition state optimization, solvent model simulations, and the ability to calculate a wide range of electronic properties.[42] Additionally, the VAMP module includes various improvements for optimizing geometry, transition states, and electrostatic interactions.[57,58] VAMP enables faster computation of molecular properties for complex systems, especially useful in initial screening and comparison with higher-level DFT outputs.

Key parameters and settings used in the VAMP calculations include:

- Hamiltonian: NDDO.
- Convergence scheme: standard.
- SCF quality: fine.
- SCF convergence: 1×10^{-6} eV.
- Spin treatment: RHF.

The electronic properties evaluated using VAMP included:

- Heat of formation.
- Ionization potential.
- HOMO–LUMO mapping and energy level gap.
- COSMO sigma profile.
- UV-visible spectral analysis.

VAMP calculations served two primary purposes:

(1) Validation: to cross-check trends and values obtained from DMol^3 (*e.g.*, ΔE_{gap}, orbital ordering).

(2) Screening: to rapidly evaluate different configurations and identify those with promising electronic characteristics for further DFT-level analysis.

2.4 Simulation of CuO and ZnO adsorption on conceptualized biochar (CBC)

The Adsorption Locator module in BIOVIA Materials Studio[45] was used to simulate the interactions between the conceptualized biochar model (CBC) and metal oxide nanonutrients (CuO and ZnO). This tool applies a Monte Carlo simulated annealing algorithm to identify thermodynamically favorable adsorption configurations between the adsorbent (biochar) and the adsorbate (nanoparticle), particularly for non-periodic systems such as amorphous or porous materials.

For each metal oxide (CuO and ZnO), 10 independent adsorption configurations were generated to capture potential variability in orientation and binding sites. The biochar model ($C_{60}H_{39}NO_{13}$) was treated as the fixed substrate, while the single CuO or ZnO served as the adsorbate. The simulation identified adsorption sites that minimized the potential energy of the complex. The force field used was COMPASS (version 2.8),

Table 1 Adsorption simulation parameters (Adsorption Locator)

Parameter	Value
Simulated annealing calculation parameters	
Loading steps	100 000
Heating cycles	5
Steps per cycle	50 000
Optimize geometry	Yes
Energy parameters	
Forcefield	COMPASS (version 2.8)
Charges	Forcefield assigned
Electrostatic terms	
Summation method	Group based
Cutoff distance	15.5 A
Buffer width	0.5 A
van der Waals terms	
Summation method	Atom based
Truncation method	Cubic spline
Cutoff distance	15.5 A
Spline width	1 A
Buffer width	0.5 A
Simulated annealing	
Automatic	Yes
Adjust Monte Carlo step sizes	Yes
Simulated annealing calculation	
Framework charge	0.000 e
Maximum adsorption distance	5.000 A

which supports a wide range of organic and inorganic systems. Table 1 summarizes the key parameters used for the simulated annealing process.

The output configurations from Adsorption Locator were further used for energy calculations and quantum-level simulations described in the next section.

2.5 Quantum chemical calculations (DFT) and electronic structure analysis

To evaluate adsorption energetics and electronic properties of the selected CBC–nanoparticle complexes, density functional theory (DFT) calculations were performed using the DMol^3 module in Materials Studio.[45] All calculations were conducted on non-periodic (cluster-based) models with the following set parameters:

Exchange–correlation: generalized gradient approximation (GGA) with PBE.

Basis set: double numerical plus polarization (DNP).

Dispersion correction: Grimme DFT-D applied.

Spin treatment: spin-unrestricted.

Boundary conditions: vacuum boundary (≥15 Å in all directions).

Convergence criteria: energy = 1×10^{-6} Ha, force = 0.002 Ha Å^{-1}, and displacement = 0.005 Å.

2.5.1 Properties computed and mathematical relationships

2.5.1.1 Adsorption energy. For the optimized biochar structure or CuO and ZnO nanoparticles, adsorption energy was computed, and the mathematical relationships are given below.

2.5.1.2 Rigid adsorption energy and deformation energy. These parameters were also computed to decouple pure interaction from structural distortion effects.

2.5.1.3 Electronic properties. HOMO and LUMO energies, energy gap (ΔE_{gap}), ionization potential, total energy, and heat of formation were calculated to assess stability and reactivity.

2.5.1.4 Orbital visualization. The spatial distribution of frontier molecular orbitals was analyzed to understand electron density localization and possible adsorption sites.

2.5.1.5 Comparative analysis. Co-adsorption simulations (ZnO and CuO together) were also conducted to evaluate competitive or synergistic effects on binding.

The Material Studio Adsorption Locator[45] module was used to carry out Monte Carlo searches for the configurationally favorable adsorbate–adsorbent system as the temperature is gradually reduced.[59] Mathematically, these parameters can be defined as:[60,61]

$$E_{ads} = E_{total} - (E_{CBC} + E_{NN}) \quad (1)$$

where E_{ads} represents the "apparent" adsorption energy (in eV), which is the energy change associated with the adsorption of a sorbate onto the sorbent surface. E_{total} represents the total energy (in eV) of the sorbate-sorbent system, which includes contributions from all components involved in the adsorption process. E_{CBC} represents the energy of the adsorbent (CBC) in isolation. E_{NN} represents the energy of the adsorbate nanonutrient (NN) in isolation.

The deformation energy (E_{deform}) can be expressed as:[56,62]

$$E_{deform} = E_{total} - E_{rigid} \quad (2)$$

where E_{rigid} represents the energy associated with the adsorption when both the sorbent and the sorbate are treated as rigid bodies where no structural changes occur during adsorption. E_{deform} represents a measure of the energy change resulting from structural adjustments of the adsorbent (CBC) or adsorbate during adsorption.

The change in adsorption energy with increasing nanonutrient concentration provides insights into system stability and interaction strength, which is mathematically defined as

$$\frac{\Delta E_{ads}}{\Delta N_i} = f(N_i) \quad (3)$$

where $f(N_i)$ represents a function that captures how adsorption energy E_{ads} varies as the number (or concentration) of nanonutrients N_i changed in the system.

In the co-presence of both nanonutrients, the overall total adsorption energy, total deformation energy and normalized adsorption energy per site can be expressed as shown in eqn (4)–(6):[56,58,62]

$$E_{ads(combined)} = E_{ads(ZnO)} + E_{ads(CuO)} \quad (4)$$

$$E_{deform(combined)} = E_{deform(ZnO)} + E_{deform(CuO)} \quad (5)$$

$$\left(\frac{\Delta E_{ads}}{\Delta N_i}\right)_{combined} = \left(\frac{\Delta E_{ads}}{\Delta N_i}\right)_{ZnO} + \left(\frac{\Delta E_{ads}}{\Delta N_i}\right)_{CuO} \quad (6)$$

3. Results and discussion

3.1 Conceptualized biochar (CBC) structure: molecular properties

This study aimed to elucidate the sorption interactions between nanonutrients and conceptualized biochar (CBC) through molecular dynamics (MD) simulations. Despite their potential, MD simulations have been underutilized in nanofertilizer formulation research, which is crucial for designing efficient nano-enabled biochar-based fertilizers. Zinc oxide (ZnO) and copper oxide (CuO) were selected as model nanonutrients due to their essential roles as micronutrients for plant health and their typical scarcity in biochar. To address this knowledge gap, we employed MD simulations to investigate the adsorption behavior of ZnO and CuO on CBC. The molecular properties of the optimized CBC structure used in this study are presented in Table 2.

A negative heat of formation of −226.45 kcal mol^{-1} indicates that the CBC molecule is thermodynamically stable compared to its constituent elements in their standard states. This chemically explains why BC is stable under ambient conditions, which is beneficial for applications like long-term carbon sequestration and soil amendment.[46,63] The highly negative electronic energy (−149 966.37 eV) typically indicates a stable electronic configuration, suggesting that the molecule has a steady arrangement of electrons. This usually implies less

Table 2 Computational data obtained using BIOVIA Material Studio software for the optimized CBC using the VAMP (Valence Atomic and Molecular Properties) module

Parameter	Values
Heat of formation	−226.45 kcal mol^{-1}
Electronic energy	−149 966.37 eV
Core–core repulsion	137 380.22 eV
Total energy	−12 586.15 eV
Gradient norm	0.38 kcal mol^{-1} $Å^{-1}$
Root mean square (RMS) force	0.02
Ionization potential	8.37 eV
Filled levels	181
Molecular weight	981.97 g mol^{-1}
SCF calculations	823

chemical reactivity since chemical reactions generally involve electrons in covalent or electrovalent systems. The ionization potential represents the energy required to remove an electron from the molecule. A higher ionization potential suggests that the molecule is relatively stable and less reactive, which may be advantageous in applications where chemical stability is desired, such as long-term carbon sequestration and soil amendments. Furthermore, the CBC with a total energy of −12 586.15 eV, which indicates the total kinetic and potential energies, showed a stable molecular structure since higher negative values indicate higher stability.[64] This is further indicated by the core–core repulsion value of 137 380.22 eV showing the repulsive interactions between core electrons in the atom. A high core–core repulsion energy indicates that the electronic structure is well-defined, further contributing to overall stability.

The gradient norm indicates how close the molecular structure is to an energy minimum during optimization calculations. A lower value (0.38) suggests that the structure is close to a local minimum, indicating stability. Similarly, the root mean square (RMS) force provides insight into the forces acting on atoms in the molecule during optimization. A low RMS (0.02) value indicates that the molecular structure is well-optimized and stable, with minimal forces acting to change its configuration. Generally, these data show that the CBC molecule is thermodynamically stable, well-optimized structurally, and has a relatively high ionization potential, suggesting low reactivity under normal conditions. These theoretical values agree with evidence of biochar's recalcitrant nature as it is not readily mineralized in the soil by either abiotic or biotic processes.[65] These characteristics are favorable for applications in soil amendment and carbon sequestration, where stability and minimal reactivity are desired attributes.

3.2 Conceptualized biochar (CBC) structure

3.2.1 Frontier molecular orbitals: lowest unoccupied molecular orbital (LUMO) and highest occupied molecular orbital (HOMO). According to Koopmans' theory of frontier molecular orbitals,[66] the energies of the highest occupied molecular orbital (E_{HOMO}) and the energy of the lowest unoccupied molecular orbital (E_{LUMO}) can represent the ionization energy (IE) and electron affinity (EA)[67] as stated in eqn (7) and (8):

$$IE = -E_{HOMO} \quad (7)$$

$$EA = -E_{LUMO} \quad (8)$$

In this case, ionization energy (IE) represents the energy needed to remove an electron from the HOMO site (Fig. 6a) and EA represents the energy needed to add an electron to a LUMO site. Typically, the lower these values, the higher the reactivity of the molecule. For the CBC, the computed values are

$$\text{Ionization energy, IE} = -E_{HOMO} = -(-0.184985\ \text{eV}) = 0.184985\ \text{eV}$$

and

$$\text{Electron affinity, EA} = -E_{LUMO} = -(-0.126879\ \text{eV}) = 0.126879\ \text{eV}.$$

Therefore, the HOMO–LUMO energy gap, ΔE_{gap}, which also indicates the tendency of the HOMO–LUMO sites to lose or gain electrons in a reaction,[58] can be calculated as

$$\Delta E_{gap} = E_{LUMO} - E_{HOMO} = -0.126879 - (-0.184985) = 0.058106\ \text{eV}$$

A small HOMO–LUMO gap (*e.g.*, 0.058106 eV in this case) typically suggests high chemical reactivity because electrons require less energy to transition from the HOMO to the LUMO. This is often associated with materials that are prone to electron transfer, making them reactive. However, biochar is generally known for its stability and low reactivity, as supported by other molecular parameters in Table 2, like low RMS force, high heat of formation, and high ionization potential.[68,69] In biochar, the HOMO and LUMO are usually localized on specific functional groups or unsaturated carbon atoms at edges with distinct spatial separation, which could reduce the energy gap without significantly affecting overall reactivity or structural stability.[70,71] For example, the HOMO may be localized on electron-donating groups while the LUMO may be localized on electron-deficient regions, such as aromatic rings (Fig. 6b). Also, oxygen-containing functional groups (*e.g.*, –OH or –COOH) can influence orbital energies, reducing the gap without necessarily increasing overall reactivity.[70,72] Overall, this localized reactivity may play a role in the adsorption process through van der Waals and π-electrons from the aromatic rings in the biochar molecule.[73]

3.2.2 UV-Vis spectral analysis. The UV-Vis spectrum provides insights into the electronic transitions occurring within the CBC molecule. Fig. 7 indicates that it does not exhibit full-spectrum absorption, with its absorption primarily occurring within the UV region. This characteristic may be desirable when biochar is utilized as a soil amendment, as it allows for heat absorption, thereby helping to regulate soil temperatures.[74,75] Such temperature regulation can benefit the soil

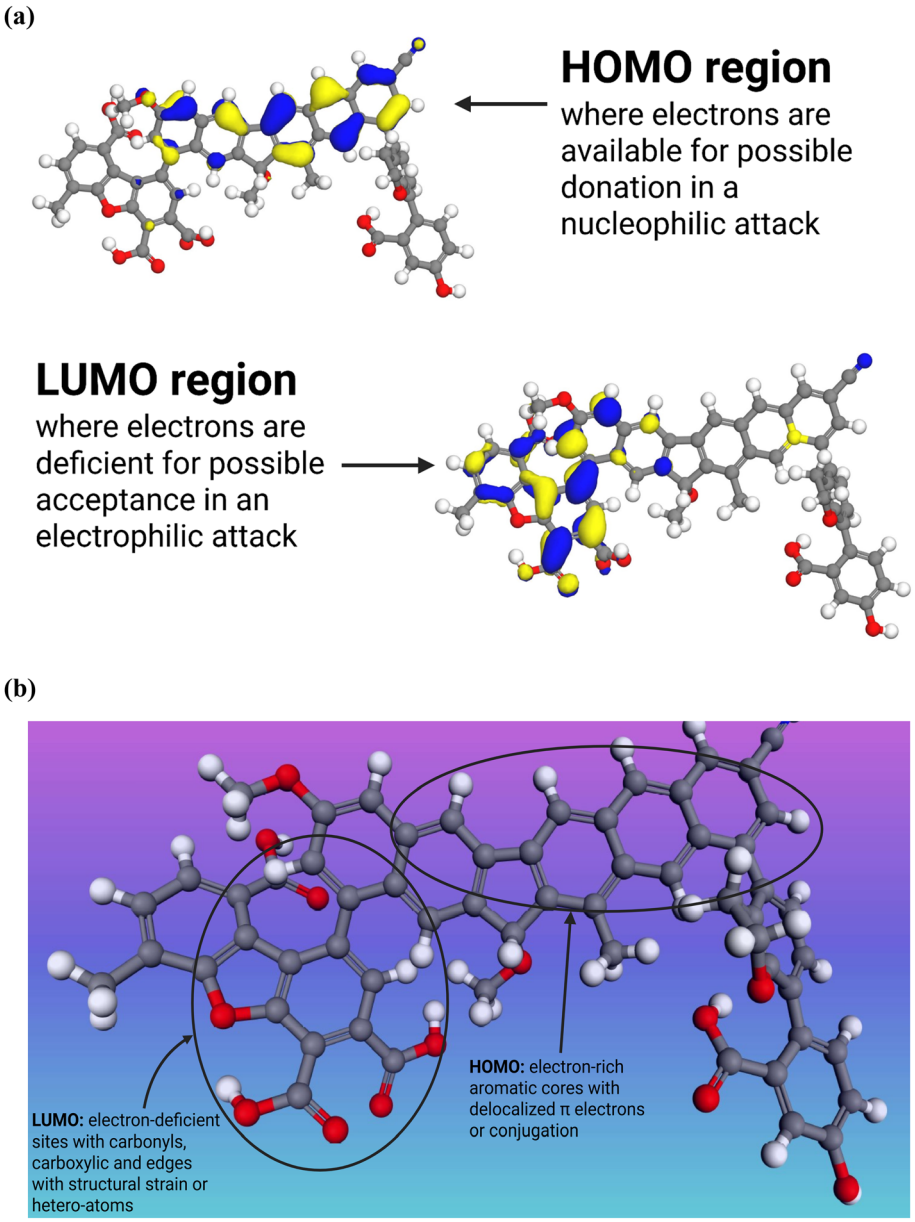

Fig. 6 (a) DMol^3 module used to analyze the CBC structure: HOMO and LUMO maps shown in distinctly different regions of the structure ($E_{HOMO} = -0.184985$ eV and $E_{LUMO} = -0.126879$ eV). (b) Atoms or groups involved in HOMO–LUMO transitions.

microbiome and, ultimately, plant health. However, as noted by Mohtaram *et al.*,[76] biochar can be enhanced through modification with photosensitive nanomaterials, which improves its light absorption capabilities beyond the UV range (10–400 nm), thereby resulting in a biochar product that is more suitable for applications in photocatalysis or solar energy capture.

3.2.3 COSMO sigma profile. The COSMO sigma profile of the conceptualized biochar (CBC) structure, as shown in Fig. 8, provides insight into the surface polarity distribution behavior of the molecule.[77] The *x*-axis represents the screening charge density (σ) in units of e Å^{-2}, while the *y*-axis denotes the surface area (σ-profile) corresponding to each σ value in Å^2. The profile exhibits a dominant peak centered near $\sigma \approx 0$ e Å^{-2}, indicating a significant proportion of the non-polar surface area.[77] This suggests that the CBC structure is largely hydrophobic in nature, a characteristic typical of carbon-rich biochar materials.

However, the presence of noticeable shoulders and peaks on both sides of the neutral region—particularly around $\sigma \approx -0.006$ to -0.012 e Å^{-2} (left/negative side) and $\sigma \approx +0.009$ to $+0.014$ e Å^{-2} (right/positive side)—implies the existence of polar functional groups capable of acting as hydrogen bond acceptors and donors, respectively.[78] The sharper peak on the positive side further supports the presence of donor-type groups, such as hydroxyl or amine functionalities, possibly formed during the biochar production. Overall, this bipolar character of the CBC structure, despite its largely non-polar surface, enhances its amphiphilic nature, making it suitable for interaction with both hydrophilic and hydrophobic species.[77,78] This is especially

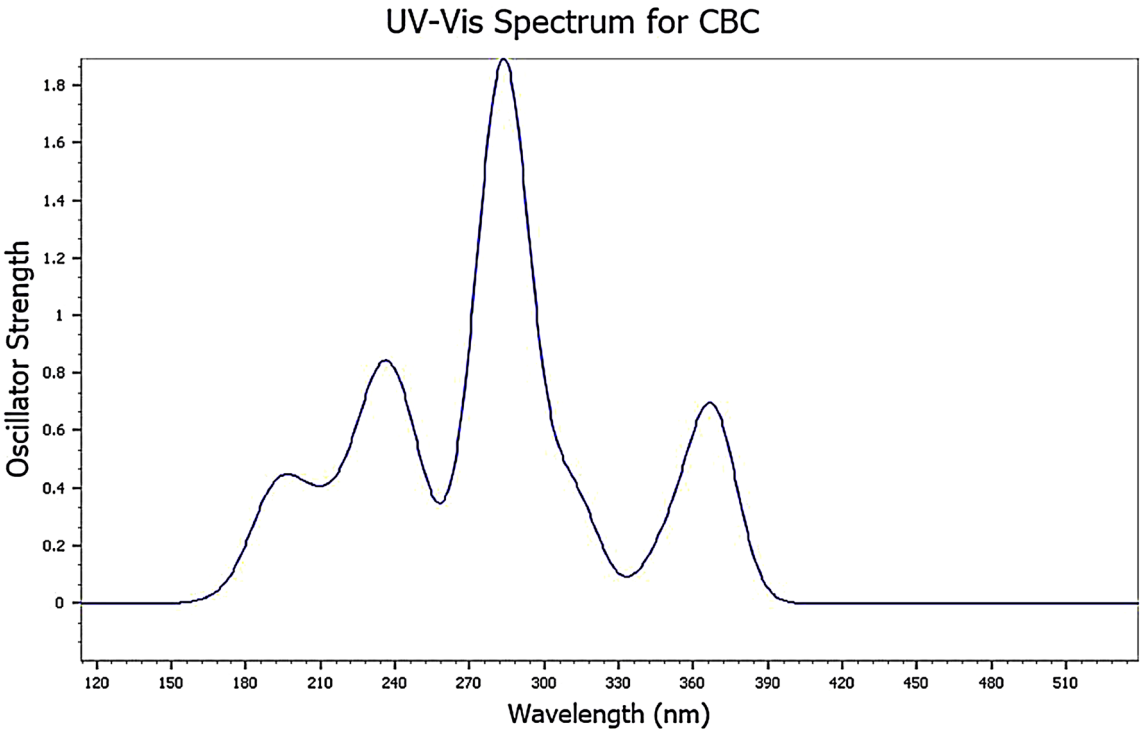

Fig. 7 UV-Vis spectrum of CBC showing feasible electronic transition peaks.

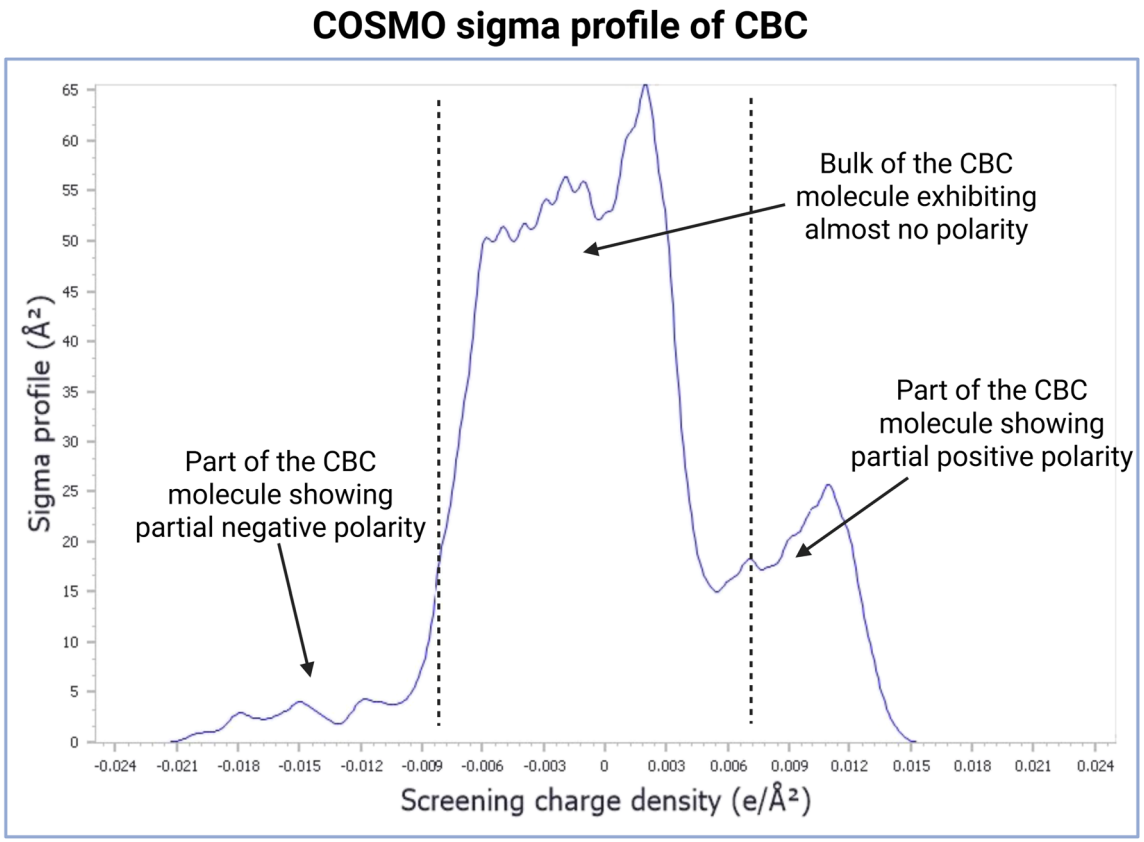

Fig. 8 COSMO sigma profile of the conceptualized biochar (CBC) structure.

relevant to adsorption processes involving polar nanonutrients such as ZnO and CuO, as highlighted in this study. Charge distribution across atoms in the CBC molecule—analyzed using Coulson and Mulliken atomic charge assignments in these computational studies—offers valuable insight into these observations (see SI data).

3.3 Computational simulation of CuO and ZnO nanonutrient adsorption on CBC

The total adsorption energies (E_{ads}) of ZnO and CuO on CBC is largely influenced by ZnO, primarily due to its higher deformation energy upon adsorption. Using configurational structure #1, for example

$$E_{ads(ZnO)} + E_{ads(CuO)} = -3072.698 + (-34.792) = -3107.490 \text{ eV}$$

Meanwhile, for the co-presence of ZnO and CuO, the simulated $E_{ads(combined)} = -2042.611$ eV. This implies that the presence of ZnO and CuO as single or co-adsorbates does not change the overall exothermic nature of the adsorption (Table 3 and Fig. 9), however, the overall adsorption energy was modulated when both NNs were co-present.

Table 3 Energetics of ZnO–CBC, CuO–CBC and co-adsorption processes

ZnO–CBC adsorption (independent)

Structures	Total energy E_{total} (eV)	Adsorption energy E_{ads} (eV)	Rigid adsorption energy E_{rigid} (eV)	Deformation energy E_{deform} (eV)	$\frac{\Delta E_{ads}}{\Delta N_i}$
Structure – 1	−3366.827	−3072.698	−1.114	−3071.584	−3072.698
Structure – 2	−2390.131	−2096.002	−0.255	−2095.747	−2096.002
Structure – 3	−1932.231	−1638.103	−2.618	−1635.485	−1638.103
Structure – 4	−332.837	−38.709	−28.355	−10.354	−38.709
Structure – 5	−327.516	−33.388	−22.959	−10.429	−33.388
Structure – 6	−325.888	−31.760	−21.170	−10.590	−31.760
Structure – 7	−323.276	−29.148	−18.478	−10.670	−29.148
Structure – 8	−321.949	−27.820	−17.269	−10.551	−27.820
Structure – 9	−320.743	−26.614	−15.925	−10.690	−26.614
Structure – 10	−318.218	−24.090	−13.385	−10.705	−24.090
Average	**−995.96**	**−701.83**	**−14.15**	**−687.68**	**−701.83**

CuO–CBC adsorption (independent)

Structures	Total energy E_{total} (eV)	Adsorption energy E_{ads} (eV)	Rigid adsorption energy E_{rigid} (eV)	Deformation energy E_{deform} (eV)	$\frac{\Delta E_{ads}}{\Delta N_i}$
Structure – 1	−252.976	−34.792	−28.634	−6.158	−34.792
Structure – 2	−248.153	−29.970	−23.801	−6.169	−29.970
Structure – 3	−245.852	−27.668	−21.387	−6.282	−27.668
Structure – 4	−243.653	−25.469	−19.155	−6.315	−25.469
Structure – 5	−242.572	−24.389	−18.125	−6.264	−24.389
Structure – 6	−240.721	−22.538	−16.185	−6.353	−22.538
Structure – 7	−238.107	−19.924	−13.553	−6.371	−19.924
Structure – 8	−237.877	−19.694	−13.342	−6.352	−19.694
Structure – 9	−236.221	−18.038	−11.668	−6.369	−18.038
Structure – 10	−235.082	−16.899	−10.517	−6.382	−16.899
Average	**−242.12**	**−23.94**	**−17.64**	**−6.3**	**−23.94**

CuO and ZnO adsorption simulation on CBC (co-presence)

Structures	Total energy (eV)	Adsorption energy (eV)	Rigid adsorption energy (eV)	Deformation energy (eV)	$\left(\frac{\Delta E_{ads}}{\Delta N_i}\right)_{ZnO}$	$\left(\frac{\Delta E_{ads}}{\Delta N_i}\right)_{CuO}$
Structure – 1	−2554.922	−2042.611	−17.100	−2025.510	−2051.660	9.049
Structure – 2	−896.085	−383.774	−375.973	−7.800	−357.128	−373.991
Structure – 3	−895.823	−383.511	−376.909	−6.602	−376.803	−355.252
Structure – 4	−890.085	−377.773	−370.386	−7.387	−371.155	−354.423
Structure – 5	−889.331	−377.019	−368.627	−8.393	−355.776	−367.992
Structure – 6	−888.417	−376.105	−368.438	−7.667	−370.711	−353.024
Structure – 7	−885.162	−372.850	−364.399	−8.451	−352.472	−367.282
Structure – 8	−884.629	−372.317	−364.724	−7.593	−350.886	−369.252
Structure – 9	−883.495	−371.183	−362.934	−8.249	−356.411	−361.836
Structure – 10	−883.358	−371.046	−363.246	−7.801	−352.168	−366.487
Average	**−1055.1**	**−542.82**	**−333.27**	**−209.55**	**−529.52**	**−326.05**

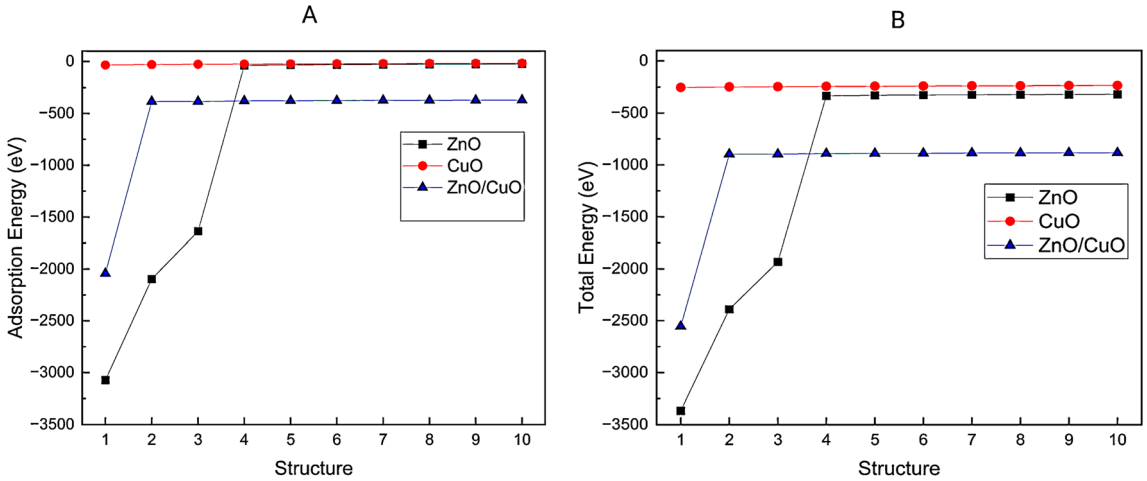

Fig. 9 Adsorption energy (E_{ads}) and total energy (E_{total}) for ZnO–CBC, CuO–CBC and [ZnO + CuO]–CBC complexes for 10 different configurational structures ((A) adsorption energy and (B) total energy).

Fig. 10 compares the deformation and rigid adsorption energies associated with the interaction of ZnO and CuO with CBC, singly and in combination. The adsorption behavior of ZnO and CuO on CBC reveals distinct interaction mechanisms. Overall average rigid adsorption energy shows that CuO may bind more strongly to CBC (−17.64 eV) than ZnO (−14.15 eV),

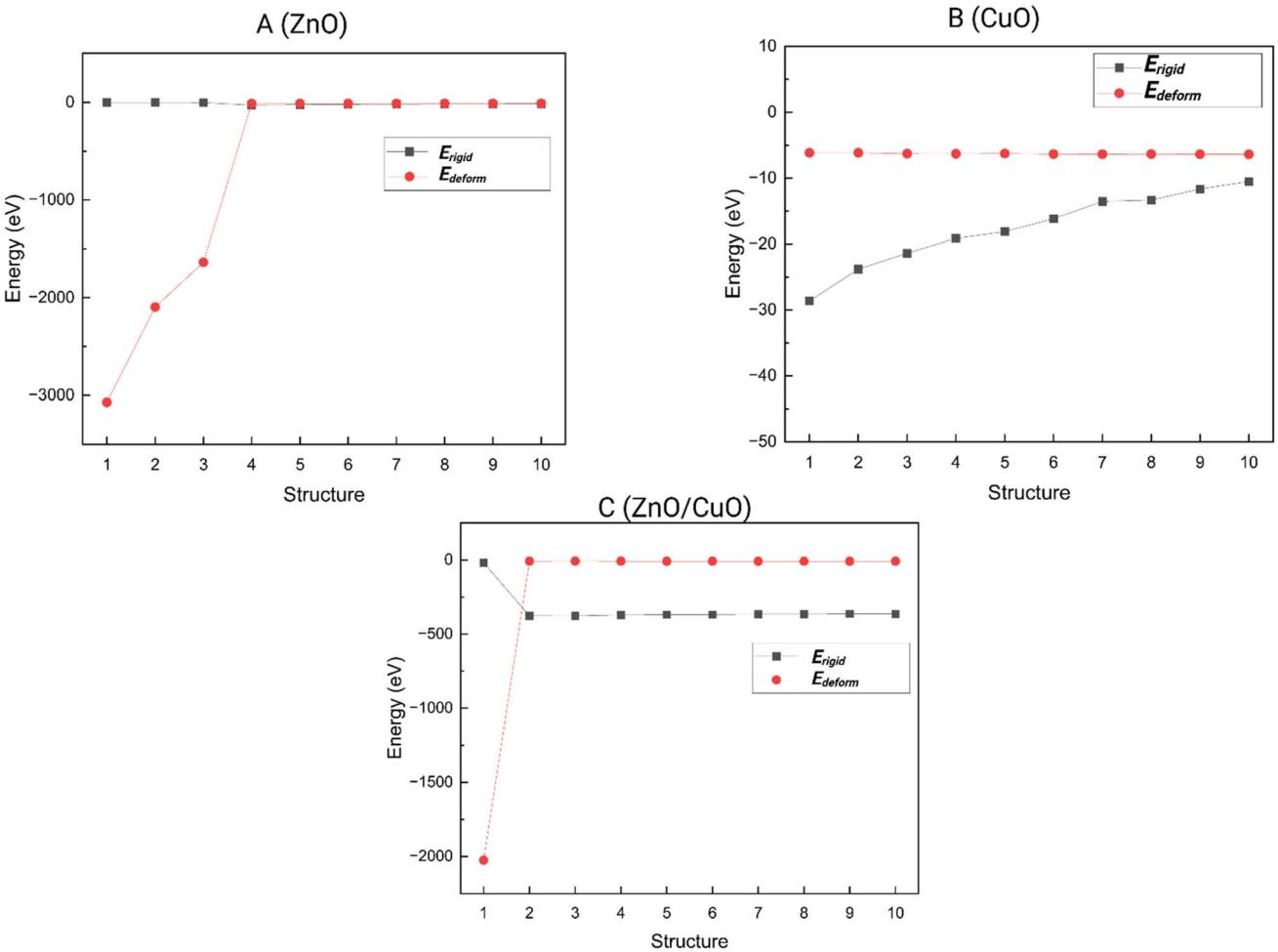

Fig. 10 Deformation energy (E_{deform}) and rigid adsorption energy (E_{rigid}) for ZnO–CBC; CuO–CBC; and (ZnO + CuO)–CBC adsorption simulations with 10 different configurational structures ((A) ZnO–CBC; (B) CuO–CBC; (C) [ZnO + CuO]–CBC).

indicating a naturally stronger affinity without requiring structural adjustment. In contrast, ZnO exhibits a higher deformation energy upon adsorption, suggesting that its interaction is strengthened through structural adaptation of both the CBC surface and the ZnO itself. This can be attributed to ZnO's shorter optimized bond length (1.561 Å *vs.* 1.717 Å for CuO), which enables it to access smaller crevices within the CBC structure, enhancing contact but also inducing strain.[79] When adsorbed together, ZnO and CuO may exhibit additive or synergistic effects, depending on site competition or cooperative binding behavior. Overall, while CuO demonstrates stronger rigid adsorption, ZnO's contribution to total adsorption is significant due to its higher deformation-driven interaction, highlighting differing but complementary adsorption characteristics or mechanisms on CBC.

Independently, adsorption energies are consistently negative across all 10 configurational structures for nano-ZnO and nano-CuO. Notably, however, for the ZnO/CuO co-adsorbate simulations, there was a striking difference. This is because in the co-present nanonutrient adsorption simulation for structure #1, the co-presence of ZnO nanonutrients actually caused extensive structural deformation, thereby pushing CuO adsorption to an endothermic process with a $\left(\frac{\Delta E_{\text{ads}}}{\Delta N_i}\right)_{\text{CuO}}$ value of +9.049 eV, whereas $\left(\frac{\Delta E_{\text{ads}}}{\Delta N_i}\right)_{\text{ZnO}}$ remains highly exothermic at −2051.660 (Table 3 and Fig. 11).

Additionally, as you move from configurational structure #1 to #10, both total energy and adsorption energy values become less negative, suggesting that later configurations may have fewer structural distortions or have weaker surface interactions (Table 3). Furthermore, the deformation energy values are relatively small, indicating that significant structural changes are not required for adsorption. As shown in Fig. 12a–c, this may imply predominantly physisorption mediated by electrostatic or van der Waals interactions.

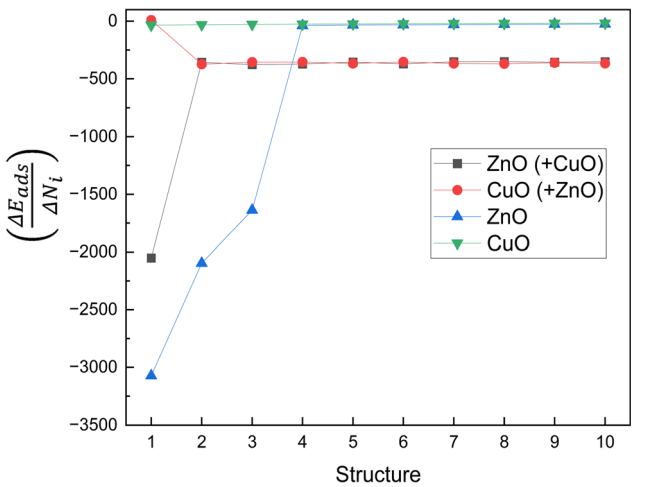

Fig. 11 Adsorption energy change with increasing nanonutrient $\frac{\Delta E_{\text{ads}}}{\Delta N_i}$ (eV) for ZnO, CuO and ZnO/CuO adsorption systems for 10 different configurational structures.

Table 4 shows a generalized comparison of the adsorption characteristics of the ZnO and CuO nanonutrients, independently, and as co-adsorbates with the CBC. The adsorption energy includes deformation energy—the energy the system spends to distort the CBC and/or adsorbate to enable binding. For ZnO, the very high deformation energy (*e.g.*, −687 eV average) indicates that the biochar structure undergoes significant structural adjustment to accommodate ZnO nanoparticles, thereby inflating the overall adsorption energy (−701.83 eV), but that does not reflect the actual adsorption strength or affinity. The rigid adsorption energy isolates the true interaction between the undistorted CBC and the adsorbate (*e.g.* CuO or ZnO), without including deformation penalties. Therefore, despite the high total system energy drop, ZnO is not binding more strongly—it only causes greater structural distortion, thereby incurring more energy costs for the overall process. This may be due to ZnO preferring more inner-pore or embedded binding modes, leading to larger structural rearrangements of the biochar matrix and hence the high deformation energy. CuO, on the other hand, may adsorb more readily on surface oxygenated groups (*e.g.*, –COOH and –OH) and the conjugated π-bonds in the aromatic rings with less structural change, resulting in a higher net rigid adsorption energy—which better reflects stronger adsorption affinity.

The rigid adsorption energies (E_{rigid}) for ZnO–CBC systems vary between −1.114 eV and −28.355 eV across the different configurations whereas CuO–CBC ranged between −10.517 eV and −28.634 eV. This shows a broader range for ZnO indicating variability in its interaction with CBC; in contrast, CuO exhibited a higher absolute value, suggesting a stronger interaction under conditions requiring fewer structural distortions. This shows that both nanomaterials can effectively interact with the CBC; however, the mechanisms and strengths vary based on the structural factors and surface properties. This observation supports the findings of Suazo-Hernández *et al.*[80] that Zn and Cu availability from soils treated with engineered ZnO and CuO nanoparticles was 597.7 and 41.8 times, respectively, compared to soils without treatments. The availability of nanonutrients in soils is a function of the quantity desorbed from the nano-conjugate, which also depends on two key factors: the quantity adsorbed and the adsorption energy. However, other extrinsic soil factors like pH, temperature, microbial activities, and cation exchange capacity could influence the desorption process and eventual nutrient availability for eventual plant nourishment. Also, Wei *et al.* observed that both nano-ZnO and nano-CuO can be readily adsorbed by activated granular sludge, but CuO-NPs were more effectively adsorbed at 1.31 g g^{-1} against 0.53 g g^{-1} for ZnO-NPs.[79] The Material Studio simulated $\frac{\Delta E_{\text{ads}}}{\Delta N_i}$ values show that as more molecules are added, there is a consistent trend toward favorable adsorption, which is crucial for understanding how these materials might behave in practical applications such as biofertilizers or nanonutrient delivery systems.[32]

When both ZnO and CuO are adsorbed together, the overall average adsorption energy is −542.82 eV. However, the individual contributions of each of nano-ZnO and nano-CuO components to the overall adsorption process in the co-

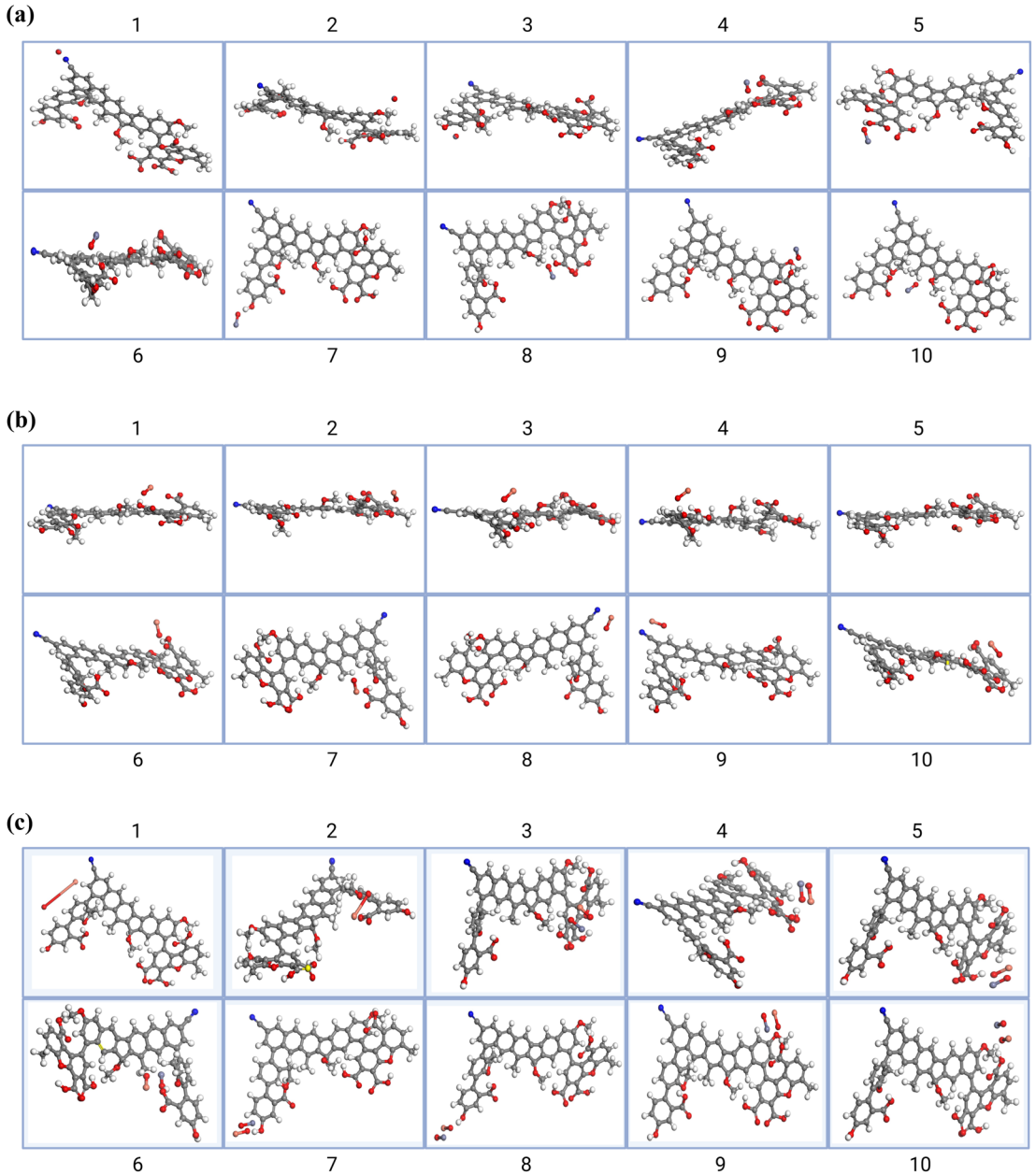

Fig. 12 (a) Different configurational structures for ZnO adsorption on CBC. (b) Different configurational structures for CuO adsorption on CBC. (c) Different configurational structures for [ZnO + CuO] adsorption on CBC (co-presence).

Table 4 Comparison of ZnO–CBC and CuO–CBC adsorption complexes

Property	ZnO–CBC	CuO–CBC	[ZnO + CuO]–CBC
Average adsorption energy	High (−701.83 eV) largely due to deformation	Very low (−23.94 eV) due to minimal deformation	Much higher than CuO and lower than ZnO (−542.82 eV)
Variation (standard deviation)	High (wide range)	Low (narrow range)	High (wide range)
Deformation energy	Higher (−687.68 eV)	Minimal (−6.3 eV)	High (−209.55 eV)
Rigid adsorption energy	Lower (−14.15 eV) indicating lower adsorption affinity	Higher (−17.64 eV) indicating higher adsorption affinity	Extremely high (−333.27 eV) indicating co-adsorption synergy
Likely binding mechanism/location	Pores or inner surfaces	Surface functional groups	Pore/inner surfaces and surface functional groups

Table 5 Comparative adsorption energies, methods, and adsorbent/adsorbate systems[a]

Adsorbent/adsorbate	Average rigid adsorption energy (eV)	Method (this work)	Literature range (eV)	Literature method	Explanation of differences between the current study and previously reported data from the literature	Reference
CBC (adsorbent)/ZnO (adsorbate)	−14.15	MC-based	−0.84	DFT-based	ZnO is adsorbed onto CBC, unlike in the literature where CO is adsorbed onto ZnO; interface effects, strong binding due to biochar surface and likely more relaxed structures	86
CBC (adsorbent)/CuO (adsorbate)	−17.64	MC-based	−1.40	DFT-based	CuO is adsorbed onto CBC, unlike in the literature, where octamethylcyclotetrasiloxane was adsorbed onto the CuO surface; a much stronger interaction expected when metal oxide clusters are adsorbed onto CBC compared to small molecules on metal oxide surfaces	83
CBC (adsorbent)/CuO & ZnO (co-adsorbates)	−333.27	MC-based	<−2 (few, indirect)	Experimental study	Synergistic and multi-site cooperative interactions significantly magnify adsorption energy in the complex CBC/ZnO + CuO co-adsorption system unlike in the literature where actual experimental work was done using tire rubber as the adsorbent for combined metal ions (Cu^{2+}, Pb^{2+} and Zn^{2+}) in wastewater solution	85

[a] (1) Literature values are predominantly based on the DFT adsorption energies of single molecules on metal oxide surfaces or experimental co-adsorption studies. (2) Present study values are obtained from Monte Carlo molecular dynamics (MC/MD) simulations, describing the adsorption of ZnO and CuO nanoparticles on conceptualized biochar (CBC). (3) Energy values are therefore not direct benchmarks but serve to illustrate methodological contrasts and emphasize the novelty of nanoparticle–biochar simulations in nanofertilizer design.

presence situation are given by $\left(\frac{\Delta E_{ads}}{\Delta N_i}\right)_{ZnO}$ and $\left(\frac{\Delta E_{ads}}{\Delta N_i}\right)_{CuO}$ with average values of −529.52 eV and −326.05 eV, respectively. Therefore, ZnO adsorption energy weakens in the presence of CuO (from −701.83 eV to −529.52 eV), whereas CuO adsorption energy strengthens significantly (from −23.94 eV to −326.05 eV). Therefore, although ZnO dominates the adsorption process due to its structural distortions on the adsorbent, its interaction with CBC is reduced in the presence of CuO while the latter benefits from ZnO co-presence by showing stronger adsorption compared to when it is alone. The data show that:

(1) ZnO has the highest adsorption energy, largely due to deformation of CBC when adsorbed alone.

(2) CuO has lower deformation energy but shows overall surface affinity with higher rigid adsorption energy.

(3) In adsorption simulations with ZnO and CuO as co-adsorbates:

(a) ZnO interaction with CBC weakens (less negative adsorption energy).

(b) CuO interaction with CBC significantly strengthens (more negative adsorption energy).

(c) The overall adsorption energy (−542.82 eV) remains closer to the ZnO individual contribution, indicating that ZnO still contributes significantly to the adsorption process.

The increase in CuO adsorption energy in the presence of ZnO suggests synergistic effects, possibly due to charge redistribution or structural changes in the CBC substrate that favor CuO adsorption in the presence of ZnO or a synergy of mechanisms. These computational data support experimental results indicating that the adsorbent's (*e.g.* activated carbon) behaviour was influenced by the co-presence and ratio of metal oxides especially ZnO and CuO.[81,82]

Furthermore, analysis of the structures depicted by Material Studio for each of the 10 configurational structures for the adsorption simulations (independently and co-presently) shows that the adsorption of the ZnO and CuO nanomaterials is typically controlled by surface electrostatic and van der Waals interactions, which indicates a strong physisorption process. Notably, for structures 1 and 2 in the co-present simulation studies, only CuO was adsorbed but for the structures from #3 to 10, both nanoparticles were adsorbed. This could be because ZnO requires high deformation energy when binding with CBC compared to CuO with less deformation energy.

Although the computed rigid adsorption energies for CuO (−17.64 eV) and ZnO (−14.15 eV) in this computational study suggest strong interactions between these metal oxides and the biochar surface, direct experimental measurements of absolute adsorption energies are uncommon. However, related thermodynamic data and experimental observations consistently show that metal–biochar composites form stable interactions. Particularly, calorimetric and adsorption studies often report adsorption or binding energies for metal oxides on carbon-based materials in the chemisorption range (typically 0.4–2.0 eV), with CuO demonstrating stronger affinity for biochar than ZnO.[83] Moreover, the enhanced interaction of Cu species with oxygenated functional groups on biochar has been confirmed by spectroscopic analysis and adsorption isotherms, supporting the trend of higher computed adsorption energy for CuO.[84,85] These findings demonstrate that, although the absolute computational values exceed previously reported ranges due to methodological differences, our qualitative results regarding the higher binding strength and adsorption of CuO relative to ZnO on biochar are consistent with available experimental observations reported in the literature. A comparative summary of adsorption energy values for CuO and ZnO on carbon-based and other systems is presented in Table 5. Literature reports generally show adsorption energies in the range of −0.4 to −1.4 eV for single adsorbates, obtained primarily from DFT simulations of small molecules on metal oxide surfaces, and values below −2.0 eV in some experimental co-adsorption studies. In contrast, the present work evaluates ZnO and CuO nanoparticle adsorbates on a conceptualized biochar (CBC) surface using Monte Carlo molecular dynamics simulations (Section 2.4). The adsorption energies reported here stem from MC/MD simulations of nanoparticle–biochar systems, which differ fundamentally from the DFT-based molecule–oxide studies common in the literature; combined with our metadata survey in the introduction showing the paucity of MD applications in nanofertilizer research, this underscores both the novelty and methodological distinction of the present work.

4. Environmental factors influencing nanoparticle–biochar interactions in soil systems

While computational simulations provide valuable insight into the intrinsic adsorption behavior of nanoparticles (NPs) on biochar surfaces, real-world soil conditions introduce significant complexity.[87] Since the primary goal is to utilize the nanofertilizer as a delivery system for nanonutrients to support plant growth,[88,89] key environmental factors—such as soil moisture, pH, ionic composition (*e.g.*, Cl^-, NO_3^-, and SO_4^{2-}), organic matter content, redox conditions, and microbial activity—play critical roles in influencing the stability, transformation, adsorption, and desorption of nanoparticles (*e.g.*, ZnO and CuO) eventually at the soil–nanofertilizer interface.[87,90] These factors cannot be overlooked, as they ultimately determine the fate and bioavailability of the nanonutrients and thus their effectiveness in nourishing plants. Here, we briefly discuss possible impacts of these factors.

4.1 Moisture and water content

Soil moisture is a primary determinant of NP behavior as hydration layers formed on biochar-based fertilizers can block or alter its nutrient release pattern, limiting direct interaction between nanonutrients from the biochar and the plant.[91,92] Water also influences dissolution; for example, ZnO nanoparticles dissolve to release Zn^{2+} more readily than CuO, affecting mobility and bioavailability. High moisture may also promote NP aggregation, reducing the effective surface area for adsorption.[93]

4.2 Soil pH

Soil pH regulates the surface charge of both biochar and nanoparticles.[93] At low pH, biochar's functional groups (such as –COOH and –OH) are protonated, diminishing their ability to bind metal oxides or ions. Under neutral to alkaline conditions, deprotonation increases negative surface charge, enhancing NP adsorption.[94] Also, pH determines the chemical speciation of ZnO and CuO, altering their reactivity in the soil.

4.3 Ionic strength/composition and salinity

Anions such as Cl^- and NO_3^- can form stable aqueous complexes with metal ions (*e.g.*, $ZnCl_4^{2-}$ and $Cu(NO_3)_2$), increasing metal solubility but reducing adsorption efficiency on biochar, potentially resulting in leaching.[95] These ions may also compete with nanoparticles for adsorption sites or displace weakly bound species. High ionic strength (from Na^+, Ca^{2+}, Cl^-, *etc.*) compresses the electrical double layer, reducing electrostatic repulsion and potentially promoting aggregation or adsorption of NPs onto biochar. Multivalent cations (*e.g.*, Ca^{2+}) can facilitate charge bridging but also compete for sorption sites. Under reducing (anaerobic) conditions, metal ions, *e.g.*, Cu^{2+}, can be transformed to less soluble forms like Cu^+ or elemental Cu, altering adsorption behavior.[96] Zinc is generally less affected by redox, though redox changes can modify biochar surface chemistry and thus its sorption capacity.[95]

4.4 Natural organic matter (NOM), soil microbiome and biotic interactions

Dissolved organic matter, abundant in most soils, can form soluble complexes with metal ions or coat biochar/NP surfaces, reducing available adsorption sites or altering surface chemistry.[97] NOM can also stabilize NPs through steric hindrance, decreasing their adsorption onto solid-phase biochar. Soil microorganisms can produce organic acids and chelators (*e.g.*, siderophores), affecting the mobility, speciation, and transformation of NPs. Microbes can alter local pH and redox conditions, directly impacting nanoparticle–biochar interactions.[98]

4.5 Implications for simulation and modeling

These environmental parameters substantially modulate nanofertilizer adsorption, often shifting interaction mechanisms from simple surface adsorption to more complex behaviors such as aggregation, dissolution, complexation, or microbial transformation.[91] To accurately predict NN–biochar–soil interactions, simulation models must reflect these dynamic, heterogeneous soil conditions. While the current study provides a literature-supported discussion of these factors and their likely impacts, we recognize the need for deeper mechanistic insights through direct modeling and simulation. To this end, a separate follow-up investigation is currently underway, which will incorporate explicit simulations of biochar–nanoparticle interactions under varying soil conditions. This ongoing work aims to build upon the foundational findings presented here.

5. Conclusion

This computational study aimed to elucidate the molecular foundations of adsorption interactions between conceptualized biochar (CBC) and nanonutrients, specifically ZnO and CuO. By analyzing CBC's properties such as heat of formation, electronic energy, total energy, HOMO–LUMO energy gap, UV-Vis spectral analysis and COSMO sigma profile, we established a comprehensive understanding of its structural stability and potential as an adsorbent. The structure was optimized with VAMP and $DMol^3$ modules using Material Studio Suite software.

The adsorption simulations revealed that both ZnO and CuO exhibit energetically favourable interactions with the CBC. Notably, ZnO displayed higher deformation energy compared to CuO, leading to more negative adsorption energies (E_{ads}). This difference suggests that ZnO might require more structural adjustments for adsorption with CBC under certain conditions.

Co-adsorption simulations involving both nanonutrients showed significantly more negative average values for total energy (E_{total}) and rigid adsorption energy (E_{rigid}), indicating enhanced stability when both are co-present. However, ZnO required more energy for the adsorption process due to higher structural deformation energies (E_{deform}). This was reflected in average $\frac{\Delta E_{ads}}{\Delta N_i}$ values of −701.83 eV as a lone adsorbate and −529.52 eV with CuO co-presence. In summary, CuO demonstrates stronger adsorption on CBC when adsorbed individually compared to ZnO (−17.64 *vs.* 14.15 eV); however, the presence of ZnO appears to enhance CuO adsorption further, likely due to stabilizing interactions between ZnO and CuO on the biochar surface. Overall adsorption energy in the co-presence scenario aligns with experimental studies showing adsorption in a mixed system shows a synergistic modulation.[99]

The configurational structures from our simulations suggest strong physisorption as the preferred mechanism over chemisorption for these systems. Physisorption typically involves intermolecular forces such as electrostatic attractions, van der Waals forces, and hydrogen bonding. Compared to chemisorption, it is usually reversible, and this can be beneficial for applications requiring controlled release or desorption processes.

Taken together, this study contributes valuable insights into how different metal oxides interact at the molecular level with biochar surfaces – a crucial aspect in designing sustainable agricultural practices that integrate nanotechnology with organic amendments in biogenic fertilizers and other applications. Our findings have significant implications for designing efficient nano-biofertilizers and other applications that leverage biochar–nanoparticle interactions. The use of biochar as an adsorbent has implications for nutrient retention in soil by reducing leaching while providing a slow release mechanism beneficial for plant growth. This approach aligns with several sustainable development goals, particularly SDG 1 (No Poverty) through circular economy within the community, SDG 2 (Zero Hunger) by enhancing food security through improved crop yields and sustainable agricultural practices, and SDG 12 (Responsible Consumption and Production) by promoting

environmentally friendly fertilizer systems. Additionally, it supports SDG 13 (Climate Action) through carbon sequestration properties inherent to biochar.

Overall, the study demonstrates a novel application of molecular dynamics to nanoparticle–biochar interactions, addressing a clear gap in nanofertilizer design research. Undoubtedly, the foundational knowledge, which has been provided in this work, is necessary for optimizing biochar-based, nano-enabled fertilizers with nanonutrients such as ZnO and CuO. Future studies, however, would focus on experimental validation of these computational results alongside investigations into the environmental factors influencing these interactions under real-world conditions.

Author contributions

Adewale T. Irewale: conceptualization; methodology; data acquisition; formal analysis and investigation; writing – original draft preparation, review and editing. Elias E. Elemike: conceptualization; methodology; supervision; validation. Christian O. Dimkpa: co-supervision; resources; writing – review and editing. Emeka E. Oguzie: conceptualization; co-supervision; funding acquisition; software; validation.

Conflicts of interest

The authors claim there are no competing interests.

Data availability

All data related to this research work are freely available upon reasonable request *via* the corresponding author.

Supplementary information is available. See DOI: **https://doi.org/10.1039/d5su00646e**.

Acknowledgements

The authors gratefully acknowledge financial support from the World Bank and the Agence Française de Développement (AFD) for financial support for the Second Africa Higher Education Centres of Excellence for Development Impact (ACE Impact) Project – P169064, IDA No. 6510-NG. The authors acknowledge Prof. Agunbiade Foluso O., Department of Chemistry, University of Lagos for his review of the draft manuscript abstract and his valuable suggestions.

References

1 R. R. Tan, Data Challenges in Optimizing Biochar-Based Carbon Sequestration, *Renewable Sustainable Energy Rev.*, 2019, **104**, 174–177, DOI: **10.1016/j.rser.2019.01.032**.

2 M. Chu, W. Tian, J. Zhao, M. Zou, Z. Lu, D. Zhang and J. Jiang, A Comprehensive Review of Capacitive Deionization Technology with Biochar-Based Electrodes: Biochar-Based Electrode Preparation, Deionization Mechanism and Applications, *Chemosphere*, 2022, **307**, 136024, DOI: **10.1016/j.chemosphere.2022.136024**.

3 A. T. Irewale, C. O. Dimkpa, E. E. Elemike and E. E. Oguzie, Water Hyacinth: Prospects for Biochar-Based, Nano-Enabled Biofertilizer Development, *Heliyon*, 2024, **10**(17), e36966, DOI: **10.1016/j.heliyon.2024.e36966**.

4 K. Nagaraju, T. N. V. K. V. Prasad, M. V. S. Naidu, M. S. Chari, Y. R. Ramu and B. R. Murthy, Exploring the Benefits of Rice Husk Waste: Synthesis and Characterization of Biochar and Nanobiochar for Agricultural and Environmental Sustainability, *Int. J. Environ. Clim. Change*, 2023, **13**(9), 715–725, DOI: **10.9734/ijecc/2023/v13i92292**.

5 N. Dutta, A. Mukhopadhyay, A. Kr. Dasgupta and K. Chakrabarti, Improved Production of Reducing Sugars from Rice Husk and Rice Straw Using Bacterial Cellulase and Xylanase Activated with Hydroxyapatite Nanoparticles, *Bioresour. Technol.*, 2014, **153**, 269–277, DOI: **10.1016/j.biortech.2013.12.016**.

6 H. A. Khan, S. R. Naqvi, M. T. Mehran, A. H. Khoja, M. B. Khan Niazi, D. Juchelková and A. Atabani, A Performance Evaluation Study of Nano-Biochar as a Potential Slow-Release Nano-Fertilizer from Wheat Straw Residue for Sustainable Agriculture, *Chemosphere*, 2021, **285**, 131382, DOI: **10.1016/J.CHEMOSPHERE.2021.131382**.

7 J. Jiang, L. Zhang, X. Wang, N. Holm, K. Rajagopalan, F. Chen and S. Ma, Highly Ordered Macroporous Woody Biochar with Ultra-High Carbon Content as Supercapacitor Electrodes, *Electrochim. Acta*, 2013, **113**, 481–489, DOI: **10.1016/j.electacta.2013.09.121**.

8 P. Chaijak and P. Michu, Modified Water Hyacinth Biochar as a Low-Cost Supercapacitor Electrode for Electricity Generation From Pharmaceutical Wastewater, *Pol. J. Environ. Stud.*, 2022, **31**(6), 5471–5475, DOI: **10.15244/pjoes/150463**.

9 F. Zhang, X. Wang, D. Yin, B. Peng, C. Tan, Y. Liu, X. Tan and S. Wu, Efficiency and Mechanisms of Cd Removal from Aqueous Solution by Biochar Derived from Water Hyacinth (*Eichornia crassipes*), *J. Environ. Manage.*, 2015, **153**, 68–73, DOI: **10.1016/j.jenvman.2015.01.043**.

10 M. Abd El-Azeim, Z. Salah and A. Hammam, Assessment of Water Hyacinth Biochar as a Soil Amendment for Sandy Soils, *J. Soil Sci. Agric. Eng.*, 2021, **12**(6), 431–444, DOI: **10.21608/jssae.2021.182662**.

11 S. Wijitkosum and P. Jiwnok, Elemental Composition of Biochar Obtained from Agricultural Waste for Soil Amendment and Carbon Sequestration, *Appl. Sci.*, 2019, **9**(19), 3980, DOI: **10.3390/app9193980**.

12 R. Xu, N. P. Qafoku, E. Van Ranst, J. Li and J. Jiang, Adsorption Properties of Subtropical and Tropical Variable Charge Soils: Implications from Climate Change and Biochar Amendment, *Adv. Agron.*, 2016, **135**, 1–58, DOI: **10.1016/bs.agron.2015.09.001**.

13 Z. Sha, Y. Bai, R. Li, H. Lan, X. Zhang, J. Li, X. Liu, S. Chang and Y. Xie, The Global Carbon Sink Potential of Terrestrial Vegetation Can Be Increased Substantially by Optimal Land Management, *Commun. Earth Environ.*, 2022, **3**(1), 8, DOI: **10.1038/s43247-021-00333-1**.

14 A. T. Irewale, E. E. Elemike, C. O. Dimkpa and E. E. Oguzie, Nano-Enabled Soil Amendments: Revolutionizing Soil

Health and Crop Productivity for Sustainable Agriculture, in *Role of Nanotechnology in Sustainable Agriculture and Food Security*, ed. S. Thakur and S. Tenney, ACS Books Publishers, 2025.

15 A. Yadav, K. Yadav and K. A. Abd-Elsalam, Nanofertilizers: Types, Delivery and Advantages in Agricultural Sustainability, *Agrochemicals*, 2023, **2**(2), 296–336, DOI: **10.3390/agrochemicals2020019**.

16 A. T. Irewale, E. E. Elemike, P. E. Aikpokpodion, R. M. Thangavelu, C. O. Dimkpa and E. E. Oguzie, Morphological and Chemical Profiling of Biochar Derived from Invasive Aquatic Weed towards Bio-Nanofertilizer Development, *RSC Sustainability*, 2025, **3**, 3947–3963, DOI: **10.1039/D5SU00052A**.

17 A. T. Irewale, E. E. Elemike, A. M. Shaik, C. O. Dimkpa and E. E. Oguzie, Theoretical and Experimental Insights into BET Surface Area and Pore Analysis of Water Hyacinth Biochar: Prospects for Efficient Bio-Nanofertilizer Development, *MRS Adv.*, 2025, **10**, 1029–1035, DOI: **10.1557/s43580-025-01248-1**.

18 E. Amdeha, Biochar-Based Nanocomposites for Industrial Wastewater Treatment *via* Adsorption and Photocatalytic Degradation and the Parameters Affecting These Processes, *Biomass Convers. Biorefin.*, 2023, **14**, 23293–23318, DOI: **10.1007/s13399-023-04512-2**.

19 G. N. G. Saritha, T. Anju and A. Kumar, Nanotechnology – Big Impact: How Nanotechnology is Changing the Future of Agriculture?, *J. Agric. Food Res.*, 2022, **10**, 100457, DOI: **10.1016/j.jafr.2022.100457**.

20 T. Hofmann, G. V. Lowry, S. Ghoshal, N. Tufenkji, D. Brambilla, J. R. Dutcher, L. M. Gilbertson, J. P. Giraldo, J. M. Kinsella, M. P. Landry, W. Lovell, R. Naccache, M. Paret, J. A. Pedersen, J. M. Unrine, J. C. White and K. J. Wilkinson, Technology Readiness and Overcoming Barriers to Sustainably Implement Nanotechnology-Enabled Plant Agriculture, *Nat. Food*, 2020, **1**(7), 416–425, DOI: **10.1038/s43016-020-0110-1**.

21 K. Neme, A. Nafady, S. Uddin and Y. B. Tola, Application of Nanotechnology in Agriculture, Postharvest Loss Reduction and Food Processing: Food Security Implication and Challenges, *Heliyon*, 2021, **7**(12), e08539, DOI: **10.1016/j.heliyon.2021.e08539**.

22 S. Garg, N. P. Rumjit and S. Roy, Smart Agriculture and Nanotechnology: Technology, Challenges, and New Perspective, *Adv. Agrochem*, 2023, **3**(2), 115–125, DOI: **10.1016/j.aac.2023.11.001**.

23 S. Singh, S. Sangwan, P. Sharma, P. Devi and M. Moond, Nanotechnology for Sustainable Agriculture: An Emerging Perspective, *J. Nanosci. Nanotechnol.*, 2021, **21**(6), 3453–3465, DOI: **10.1166/jnn.2021.19012**.

24 S. Vaidya, C. Deng, Y. Wang, N. Zuverza-Mena, C. Dimkpa and J. C. White, Nanotechnology in Agriculture: A Solution to Global Food Insecurity in a Changing Climate?, *NanoImpact*, 2024, **34**, 100502, DOI: **10.1016/j.impact.2024.100502**.

25 A. T. Irewale, C. Dimkpa, F. O. Agunbiade, O. A. Oyetunde, E. E. Elemike and E. E. Oguzie, Unlocking Sustainable Agricultural Development in Africa *via* Bio-Nanofertilizer Application-Challenges, Opportunities and Prospects, *Sci. Afr.*, 2024, **25**, e02276, DOI: **10.1016/j.sciaf.2024.e02276**.

26 Z. Hu and L. Wei, Review on Characterization of Biochar Derived from Biomass Pyrolysis *via* Reactive Molecular Dynamics Simulations, *J. Compos. Sci.*, 2023, **7**(9), 354, DOI: **10.3390/jcs7090354**.

27 Y. L. Yaphary, M. He, G. Lu, F. Zou, P. Liu, D. C. W. Tsang and Z. Leng, Experiment and Multiscale Molecular Simulations on the Cu Absorption by Biochar-Modified Asphalt: An Insight into Removal Capability and Mechanism of Heavy Metals from Stormwater Runoff, *Chem. Eng. J.*, 2023, **462**, 142205, DOI: **10.1016/j.cej.2023.142205**.

28 A. Minervino and K. D. Belfield, Review of Recent Computational Research on the Adsorption of PFASs with a Variety of Substrates, *Int. J. Mol. Sci.*, 2024, **25**(6), 3445, DOI: **10.3390/ijms25063445**.

29 B. Gautam, *Homology Molecular Modeling – Perspectives and Applications*, ed. R. Trindade Maia, R. Maciel de Moraes Filho and M. Campos, IntechOpen, 2021, DOI: **10.5772/intechopen.91624**.

30 D. Bálint and L. Jäntschi, Comparison of Molecular Geometry Optimization Methods Based on Molecular Descriptors, *Mathematics*, 2021, **9**(22), 2855, DOI: **10.3390/math9222855**.

31 C. O. Dimkpa, Soil Properties Influence the Response of Terrestrial Plants to Metallic Nanoparticles Exposure, *Curr. Opin. Environ. Sci. Health*, 2018, **6**, 1–8, DOI: **10.1016/j.coesh.2018.06.007**.

32 A. K. Bhardwaj, G. Arya, R. Kumar, L. Hamed, H. Pirasteh-Anosheh, P. Jasrotia, P. L. Kashyap and G. P. Singh, Switching to Nanonutrients for Sustaining Agroecosystems and Environment: The Challenges and Benefits in Moving up from Ionic to Particle Feeding, *J. Nanobiotechnol.*, 2022, **20**(1), 19, DOI: **10.1186/s12951-021-01177-9**.

33 S. Kabiri, F. Degryse, D. N. H. Tran, R. C. da Silva, M. J. McLaughlin and D. Losic, Graphene Oxide: A New Carrier for Slow Release of Plant Micronutrients, *ACS Appl. Mater. Interfaces*, 2017, **9**(49), 43325–43335, DOI: **10.1021/acsami.7b07890**.

34 C. Tarafder, M. Daizy, Md. M. Alam, Md. R. Ali, Md. J. Islam, R. Islam, Md. S. Ahommed, M. Aly Saad Aly and Md. Z. H. Khan, Formulation of a Hybrid Nanofertilizer for Slow and Sustainable Release of Micronutrients, *ACS Omega*, 2020, **5**(37), 23960–23966, DOI: **10.1021/acsomega.0c03233**.

35 C. O. Dimkpa, J. Fugice, U. Singh and T. D. Lewis, Development of Fertilizers for Enhanced Nitrogen Use Efficiency – Trends and Perspectives, *Sci. Total Environ.*, 2020, **731**, 139113, DOI: **10.1016/J.SCITOTENV.2020.139113**.

36 R. Raliya, V. Saharan, C. Dimkpa and P. Biswas, Nanofertilizer for Precision and Sustainable Agriculture: Current State and Future Perspectives, *J. Agric. Food Chem.*, 2018, **66**(26), 6487–6503, DOI: **10.1021/acs.jafc.7b02178**.

37 C. O. Dimkpa and P. S. Bindraban, Nanofertilizers: New Products for the Industry?, *J. Agric. Food Chem.*, 2018, **66**(26), 6462–6473, DOI: 10.1021/acs.jafc.7b02150.

38 A. T. Irewale, E. E. Elemike, C. O. Dimkpa and E. E. Oguzie, Nano-Enabled Soil Amendments: Revolutionizing Soil Health and Crop Productivity for Sustainable Agriculture, *Role of Nanotechnology in Sustainable Agriculture and Food Security*, ed. S. Thakur and S. Tenney, ACS Symposium Books Series, 2025, in press.

39 G. Brundtland, *WCED: Our Common Future*, Oxford Paperbacks, 1987.

40 S. Z. Mousavi, H. R. Shadman, M. Habibi, M. Didandeh, A. Nikzad, M. Golmohammadi, R. Maleki, W. A. Suwaileh, A. Khataee, M. Zargar and A. Razmjou, Elucidating the Sorption Mechanisms of Environmental Pollutants Using Molecular Simulation, *Ind. Eng. Chem. Res.*, 2023, **62**(8), 3373–3393, DOI: 10.1021/acs.iecr.2c02333.

41 S. Sharma, P. Kumar and R. Chandra, Overview of BIOVIA Materials Studio, LAMMPS, and GROMACS, in *Molecular Dynamics Simulation of Nanocomposites Using BIOVIA Materials Studio, Lammps and Gromacs*, Elsevier, 2019, pp. 39–100, DOI: 10.1016/B978-0-12-816954-4.00002-4.

42 S. Sharma, P. Kumar and R. Chandra, Applications of BIOVIA Materials Studio, LAMMPS, and GROMACS in Various Fields of Science and Engineering, in *Molecular Dynamics Simulation of Nanocomposites Using BIOVIA Materials Studio, Lammps and Gromacs*, Elsevier, 2019, pp. 329–341, DOI: 10.1016/B978-0-12-816954-4.00007-3.

43 S. Z. Mousavi, H. R. Shadman, M. Habibi, M. Didandeh, A. Nikzad, M. Golmohammadi, R. Maleki, W. A. Suwaileh, A. Khataee, M. Zargar and A. Razmjou, Elucidating the Sorption Mechanisms of Environmental Pollutants Using Molecular Simulation, *Ind. Eng. Chem. Res.*, 2023, **62**(8), 3373–3393, DOI: 10.1021/acs.iecr.2c02333.

44 S. A. Hollingsworth and R. O. Dror, Molecular Dynamics Simulation for All, *Neuron*, 2018, **99**(6), 1129–1143, DOI: 10.1016/j.neuron.2018.08.011.

45 *BIOVIA Material Science Studio Academic Research Suite: Adsorption Locator, Forcite, DMol^3, and VAMP*, Dassault Systèmes, San Diego, 2022.

46 L. C. A. Melo, C. A. Silva, M. Á. Sánchez-Monedero, K. Jindo, S. Taherymoosavi and S. Joseph, Biochar-Based Fertilizers, Co-Composting, and Growing Media, in *Biochar for Environmental Management*, Routledge, London, 2024, pp. 669–694, DOI: 10.4324/9781003297673-26.

47 S. Xu, J. Chen, H. Peng, S. Leng, H. Li, W. Qu, Y. Hu, H. Li, S. Jiang, W. Zhou and L. Leng, Effect of Biomass Type and Pyrolysis Temperature on Nitrogen in Biochar, and the Comparison with Hydrochar, *Fuel*, 2021, **291**, 120128, DOI: 10.1016/j.fuel.2021.120128.

48 B. Chen, D. Zhou and L. Zhu, Transitional Adsorption and Partition of Nonpolar and Polar Aromatic Contaminants by Biochars of Pine Needles with Different Pyrolytic Temperatures, *Environ. Sci. Technol.*, 2008, **42**(14), 5137–5143, DOI: 10.1021/es8002684.

49 L. Bottezini, D. P. Dick, A. Wisniewski, H. Knicker and I. S. C. Carregosa, Phosphorus Species and Chemical Composition of Water Hyacinth Biochars Produced at Different Pyrolysis Temperature, *Bioresour. Technol. Rep.*, 2021, **14**, 100684, DOI: 10.1016/j.biteb.2021.100684.

50 N. Zhao, Y. Lv and X. Yang, A New 3D Conceptual Structure Modeling of Biochars by Molecular Mechanic and Molecular Dynamic Simulation, *J. Soils Sediments*, 2017, **17**(3), 641–655, DOI: 10.1007/s11368-015-1308-y.

51 X. Dong, Y. Chu, Z. Tong, M. Sun, D. Meng, X. Yi, T. Gao, M. Wang and J. Duan, Mechanisms of Adsorption and Functionalization of Biochar for Pesticides: A Review, *Ecotoxicol. Environ. Saf.*, 2024, **272**, 116019, DOI: 10.1016/j.ecoenv.2024.116019.

52 S. Qin, H. Fan, L. Jia, Y. Jin, Z. Li and B. Fan, Molecular Structure Analysis and Mercury Adsorption Mechanism of Iron-Based Modified Biochar, *Energy Fuels*, 2022, **36**(6), 3184–3200, DOI: 10.1021/acs.energyfuels.1c03832.

53 Z.-W. Tao, H.-Y. Zou, H.-H. Li, B. Wang and W.-J. Chen, Theoretical Study on the Structures and Stabilities of $CunZn_3O_3$ (n = 1–4) Clusters: Sequential Doping of Zn_3O_3 Cluster with Cu Atoms, *Inorganics*, 2024, **12**(2), 56, DOI: 10.3390/inorganics12020056.

54 T. Chen, G. Cao, Y. Qiang, Y. Lu, R. Qin, W. Xu, Y. Xie and R. Mao, Effective Removal of Pb (II) from Wastewater by Zinc-Iron Bimetallic Oxide-Modified Walnut Shell Biochar: A Combined Experimental and DFT Calculation Approach, *J. Environ. Manage.*, 2024, **370**, 122757, DOI: 10.1016/j.jenvman.2024.122757.

55 Q. Chen, J. Zheng, J. Xu, Z. Dang and L. Zhang, Insights into Sulfamethazine Adsorption Interfacial Interaction Mechanism on Mesoporous Cellulose Biochar: Coupling DFT/FOT Simulations with Experiments, *Chem. Eng. J.*, 2019, **356**, 341–349, DOI: 10.1016/j.cej.2018.09.055.

56 Nugraha, A. G. Saputro, M. K. Agusta, B. Yuliarto, H. K. Dipojono, F. Rusydi and R. Maezono, Selectivity of CO and NO Adsorption on ZnO (0002) Surfaces: A DFT Investigation, *Appl. Surf. Sci.*, 2017, **410**, 373–382, DOI: 10.1016/j.apsusc.2017.03.009.

57 P. Pourhakkak, M. Yarahmadi, E. Molaakbari, M. Aallaei, A. Alipour and A. B. Mahallati, Molecular Dynamics Simulation and Adsorption Study of Different Anticoagulants on Fullerene, *Int. J. New Chem.*, 2024, **11**(4), 469–488.

58 K. J. Uwakwe, P. C. Okafor, A. I. Obike and A. I. Ikeuba, Molecular Dynamics Simulations and Quantum Chemical Calculations for the Adsorption of Some Imidazoline Derivatives on Iron Surface, *Global J. Pure Appl. Sci.*, 2017, **23**(1), 69, DOI: 10.4314/gjpas.v23i1.8.

59 S. Sharma, P. Kumar and R. Chandra, Overview of BIOVIA Materials Studio, LAMMPS, and GROMACS, in *Molecular Dynamics Simulation of Nanocomposites Using BIOVIA Materials Studio, Lammps and Gromacs*, ed. S. Sharma, Elsevier, 2019, pp. 39–100, DOI: 10.1016/B978-0-12-816954-4.00002-4.

60 J. Lan, A. Palizhati, M. Shuaibi, B. M. Wood, B. Wander, A. Das, M. Uyttendaele, C. L. Zitnick and Z. W. Ulissi, AdsorbML: A Leap in Efficiency for Adsorption Energy Calculations Using Generalizable Machine Learning

Potentials, *npj Comput. Mater.*, 2023, **9**(1), 172, DOI: **10.1038/s41524-023-01121-5**.

61 F. E. Abeng, A. Thakur, V. C. Anadebe and E. E. Ebenso, A Comparative Density Functional Theory (DFT) and Molecular Dynamics Study on Natamycin and Cefmetazole as Effective Corrosion Inhibitor for Mild Steel: Electronic Properties and Adsorption Behavior, *Comput. Theor. Chem.*, 2025, **1248**, 115200, DOI: **10.1016/j.comptc.2025.115200**.

62 J. Yan, W. Dai, D. Zou, H. Sun, C. Tang and Y. Gui, A TMO-ZnO Heterojunction-Based Sensor for Transformer Defect Detection: A DFT Study, *Nanomaterials*, 2025, **15**(11), 856, DOI: **10.3390/nano15110856**.

63 J. Ordonez-Loza, H. Bamdad, S. Spataro, S. Papari and F. Berruti, Self-Energized Pyrolysis Process for Sustainable Biochar Production, *Energy Fuels*, 2024, **38**(20), 19598–19610, DOI: **10.1021/acs.energyfuels.4c03039**.

64 G. Ayub, N. Rahman, M. Husain, M. Sohail, R. Khan, N. Sfina, M. Elhadi, A. Azzouz-Rached and A. Alotaibi, Tailoring the Structural, Elastic, Electronic, and Optical Properties of Cs_2ScCuX_6 (X = Cl and F) Double Perovskite Compounds *via* Density Functional Theory (DFT), *J. Phys. Chem. Solids*, 2024, **188**, 111942, DOI: **10.1016/j.jpcs.2024.111942**.

65 J. Lehmann, S. Abiven, E. Azzi, Y. Fang, B. P. Singh, S. Sohi, C. Sundberg, D. Woolf and A. R. Zimmerman, Persistence of Biochar, in *Biochar for Environmental Management*, Routledge, London, 2024, pp. 277–311, DOI: **10.4324/9781003297673-11**.

66 R. Laplaza, C. Cárdenas, P. Chaquin, J. Contreras-García and P. W. Ayers, Orbital Energies and Nuclear Forces in DFT: Interpretation and Validation, *J. Comput. Chem.*, 2021, **42**(5), 334–343, DOI: **10.1002/jcc.26459**.

67 K. J. Uwakwe, P. C. Okafor, A. I. Obike and A. I. Ikeuba, Molecular Dynamics Simulations and Quantum Chemical Calculations for the Adsorption of Some Imidazoline Derivatives on Iron Surface, *Global J. Pure Appl. Sci.*, 2017, **23**(1), 69, DOI: **10.4314/gjpas.v23i1.8**.

68 G. Loebsack, K. K.-C. Yeung, F. Berruti and N. B. Klinghoffer, Impact of Biochar Physical Properties on Adsorption Mechanisms for Removal of Aromatic Aqueous Contaminants in Water, *Biomass Bioenergy*, 2025, **194**, 107617, DOI: **10.1016/j.biombioe.2025.107617**.

69 K. I. Williamson, D. J. C. Herr and Y. Mo, Mapping the Correlations between Bandgap, HOMO, and LUMO Trends for Meta Substituted Zn-MOFs, *J. Comput. Chem.*, 2024, **45**(25), 2119–2127, DOI: **10.1002/jcc.27432**.

70 Q. Su, F. Ren, M. Lu, J. Zhao, X. Zhu, T. Shen, Y. Shen, Y. Wang and J. Liang, Theoretical Study of the NO Reduction Mechanism on Biochar Surfaces Modified by Li and Na Single Adsorption and OH Co-Adsorption, *Molecules*, 2024, **29**(3), 574, DOI: **10.3390/molecules29030574**.

71 Y. Ruiz-Morales, HOMO–LUMO Gap as an Index of Molecular Size and Structure for Polycyclic Aromatic Hydrocarbons (PAHs) and Asphaltenes: A Theoretical Study. I, *J. Phys. Chem. A*, 2002, **106**(46), 11283–11308, DOI: **10.1021/jp021152e**.

72 A. Qureashi, A. H. Pandith, A. Bashir, L. A. Malik, T. Manzoor, F. A. Sheikh, K. Fatima and Z. Haq, Electrochemical Analysis of Glyphosate Using Porous Biochar Surface Corrosive NZVI Nanoparticles, *Nanoscale Adv.*, 2023, **5**(3), 742–755, DOI: **10.1039/D2NA00610C**.

73 T. Hao, Q. Zhou, J. Jiang, H. Song, Y. Pan and D. Shi, Density Functional Theory Study on the Microscopic Mechanism of NO_2 Adsorption and Reduction by Potassium-Doped Biochar: The Key Role of the Active Sites, *Biochar*, 2025, **7**(1), 67, DOI: **10.1007/s42773-025-00449-z**.

74 V. D. Rajput, A. Kumari, S. K. Upadhyay, T. Minkina, S. Mandzhieva, A. Ranjan, S. Sushkova, M. Burachevskaya, P. Rajput, E. Konstantinova, J. Singh and K. K. Verma, Can Nanomaterials Improve the Soil Microbiome and Crop Productivity?, *Agriculture*, 2023, **13**(2), 231, DOI: **10.3390/agriculture13020231**.

75 V. K. Upadhayay, M. K. Chitara, D. Mishra, M. N. Jha, A. Jaiswal, G. Kumari, S. Ghosh, V. K. Patel, M. G. Naitam, A. K. Singh, N. Pareek, G. Taj, D. Maithani, A. Kumar, H. Dasila and A. Sharma, Synergistic Impact of Nanomaterials and Plant Probiotics in Agriculture: A Tale of Two-Way Strategy for Long-Term Sustainability, *Front. Microbiol.*, 2023, **14**, DOI: **10.3389/fmicb.2023.1133968**.

76 S. Mohtaram, M. Sina Mohtaram, S. Sabbaghi, X. You, W. Wu and N. Golsanami, Enhancement Strategies in CO_2 Conversion and Management of Biochar Supported Photocatalyst for Effective Generation of Renewable and Sustainable Solar Energy, *Energy Convers. Manage.*, 2024, **300**, 117987, DOI: **10.1016/j.enconman.2023.117987**.

77 N. Elboughdiri, H. Ferkous, K. Rouibah, A. Boublia, A. Delimi, K. K. Yadav, A. Erto, D. Ghernaout, A. A. M. Salih, M. Benaissa and Y. Benguerba, Comprehensive Investigation of Cu^{2+} Adsorption from Wastewater Using Olive-Waste-Derived Adsorbents: Experimental and Molecular Insights, *Int. J. Mol. Sci.*, 2024, **25**(2), 1028, DOI: **10.3390/ijms25021028**.

78 L. Y. Ee, Y. K. Tan, J. Miao, H. T. Chu and S. F. Y. Li, High-Purity Lignin from Selective Biomass Fractionation with Ternary Deep Eutectic Solvents, *Green Chem.*, 2023, **25**(8), 3137–3151, DOI: **10.1039/D3GC00080J**.

79 L. Wei, J. Ding, M. Xue, K. Qin, S. Wang, M. Xin, J. Jiang and Q. Zhao, Adsorption Mechanism of ZnO and CuO Nanoparticles on Two Typical Sludge EPS: Effect of Nanoparticle Diameter and Fractional EPS Polarity on Binding, *Chemosphere*, 2019, **214**, 210–219, DOI: **10.1016/j.chemosphere.2018.09.093**.

80 J. Suazo-Hernández, E. Sans-Serramitjana, M. de la Luz Mora, B. Fuentes, M. de los Ángeles Sepúlveda, J. Silva-Yumi, S. Celletti, L. Celi, S. Rivas and A. Ruiz, Assessment of the Effects of ZnO and CuO Engineered Nanoparticles on Physicochemical Properties of Volcanic Ash Soil and Phosphorus Availability, *Environments*, 2024, **11**(9), 208, DOI: **10.3390/environments11090208**.

81 M. Balsamo, S. Cimino, G. de Falco, A. Erto and L. Lisi, ZnO–CuO Supported on Activated Carbon for H_2S Removal at Room Temperature, *Chem. Eng. J.*, 2016, **304**, 399–407, DOI: **10.1016/j.cej.2016.06.085**.

82 T. Yu, Z. Chen, Y. Wang and J. Xu, Synthesis of ZnO–CuO and ZnO–Co_3O_4 Materials with Three-Dimensionally Ordered Macroporous Structure and its H_2S Removal Performance at Low-Temperature, *Processes*, 2021, **9**(11), 1925, DOI: **10.3390/pr9111925**.

83 Z. Yang, Z. Chen, H. Gong and X. Wang, Copper Oxide Modified Activated Carbon for Enhanced Adsorption Performance of Siloxane: An Experimental and DFT Study, *Appl. Surf. Sci.*, 2022, **601**, 154200, DOI: **10.1016/j.apsusc.2022.154200**.

84 L.-J. Ma, T. Han, J. Jia and H.-S. Wu, Cooperative Physisorption and Chemisorption of Hydrogen on Vanadium-Decorated Benzene, *RSC Adv.*, 2020, **10**(62), 37770–37778, DOI: **10.1039/D0RA06057G**.

85 F. Cherono, N. Mburu and B. Kakoi, Adsorption of Lead, Copper and Zinc in a Multi-Metal Aqueous Solution by Waste Rubber Tires for the Design of Single Batch Adsorber, *Heliyon*, 2021, **7**(11), e08254, DOI: **10.1016/j.heliyon.2021.e08254**.

86 Z. Ni, S. Bao and X.-Q. Gong, A DFT Study of the CO Adsorption and Oxidation at ZnO Surfaces and Its Implication for CO Detection, *Chin. Chem. Lett.*, 2020, **31**(6), 1674–1679, DOI: **10.1016/j.cclet.2019.10.027**.

87 Y. Li, C. Ge, C. Cheng, X. Wang, D. Si, C. Mu, M. Wang, H. Li and D. Zhou, Nano-Biochar Uptake and Translocation by Plants: Assessing Environmental Fate and Food Chain Risk, *Sci. Total Environ.*, 2023, **905**, 167012, DOI: **10.1016/j.scitotenv.2023.167012**.

88 C. Larue, C. Baratange, D. Vantelon, H. Khodja, S. Surblé, A. Elger and M. Carrière, Influence of Soil Type on TiO_2 Nanoparticle Fate in an Agro-Ecosystem, *Sci. Total Environ.*, 2018, **630**, 609–617, DOI: **10.1016/j.scitotenv.2018.02.264**.

89 A. El-Henawy, I. El-Sheikh, A. Hassan, A. Madein, A. El-Sheikh, A. El-Yamany, A. Radwan, F. Mohamed, M. Khamees, M. Ramadan, M. Abdelhamid, H. Khaled, H. El-Faramawy, Y. Ayoub, S. Youssef and S. E.-D. Faizy, Response of Cultivated Broccoli and Red Cabbage Crops to Mineral, Organic and Nano-Fertilizers, *Env. Biodivers. Soil Secur.*, 2018, **2**(2018), 1–25, DOI: **10.21608/jenvbs.2019.6797.1046**.

90 V. Yamini, V. Shanmugam, M. Rameshpathy, G. Venkatraman, G. Ramanathan, H. AL Garalleh, A. Hashmi, K. Brindhadevi and V. Devi Rajeswari, Environmental Effects and Interaction of Nanoparticles on Beneficial Soil and Aquatic Microorganisms, *Environ. Res.*, 2023, **236**, 116776, DOI: **10.1016/j.envres.2023.116776**.

91 X. Gao, S. M. Rodrigues, E. Spielman-Sun, S. Lopes, S. Rodrigues, Y. Zhang, A. Avellan, R. M. B. O. Duarte, A. Duarte, E. A. Casman and G. V. Lowry, Effect of Soil Organic Matter, Soil pH, and Moisture Content on Solubility and Dissolution Rate of CuO NPs in Soil, *Environ. Sci. Technol.*, 2019, **53**(9), 4959–4967, DOI: **10.1021/acs.est.8b07243**.

92 M. Ahmad, A. U. Rajapaksha, J. E. Lim, M. Zhang, N. Bolan, D. Mohan, M. Vithanage, S. S. Lee and Y. S. Ok, Biochar as a Sorbent for Contaminant Management in Soil and Water: A Review, *Chemosphere*, 2014, **99**, 19–33, DOI: **10.1016/j.chemosphere.2013.10.071**.

93 A. Anderson, J. McLean, P. McManus and D. Britt, Soil Chemistry Influences the Phytotoxicity of Metal Oxide Nanoparticles, *Int. J. Nanotechnol.*, 2017, **14**(1/2/3/4/5/6), 15, DOI: **10.1504/IJNT.2017.082438**.

94 S. Jiang, L. Huang, T. A. H. Nguyen, Y. S. Ok, V. Rudolph, H. Yang and D. Zhang, Copper and Zinc Adsorption by Softwood and Hardwood Biochars under Elevated Sulphate-Induced Salinity and Acidic pH Conditions, *Chemosphere*, 2016, **142**, 64–71, DOI: **10.1016/j.chemosphere.2015.06.079**.

95 T. H. DeLuca, M. J. Gundale, M. D. MacKenzie, S. Gao and D. L. Jones, Biochar Effects on Soil Nutrient Transformations, in *Biochar for Environmental Management*, Routledge, London, 2024, pp. 401–440, DOI: **10.4324/9781003297673-16**.

96 A. Rodríguez-Seijo, C. Soares, S. Ribeiro, B. F. Amil, C. Patinha, A. Cachada, F. Fidalgo and R. Pereira, Nano-Fe_2O_3 as a Tool to Restore Plant Growth in Contaminated Soils – Assessment of Potentially Toxic Elements (Bio) Availability and Redox Homeostasis in *Hordeum Vulgare* L., *J. Hazard. Mater.*, 2022, **425**, 127999, DOI: **10.1016/j.jhazmat.2021.127999**.

97 S. H. Bai, M. B. Farrar, M. Gallart, F. Reverchon, S. Taherymoosavi, N. Omidvar, E. Kichamu-Wachira and S. Joseph, Biochar Effects on Nutrient Leaching, in *Biochar for Environmental Management*, Routledge, London, 2024, pp. 489–511, DOI: **10.4324/9781003297673-19**.

98 J. J. Pignatello, M. Uchimiya and S. Abiven, Aging of Biochar in Soils and Its Implications, in *Biochar for Environmental Management*, Routledge, London, 2024, pp. 249–276, DOI: **10.4324/9781003297673-10**.

99 J. M. Tharayil, P. Chinnaiyan, B. Ramasamy and A. Sathasivan, Biogenic Synthesis of Cu/ZnO Functionalized Biochar Composite: A Sustainable Approach for Visible Light-Photocatalytic Degradation, *Environ. Technol. Innovation*, 2025, **39**, 104337, DOI: **10.1016/j.eti.2025.104337**.